THERMAL FLUCTUATION AND EXCESS CONDUCTIVITY PROPERTIES OF YBCO-ADDED CHITOSAN, CaO AND Ca COMPOUND

By

YAP SIEW HONG

Thesis Submitted to the School of Graduate Studies, Universiti Putra Malaysia, in Fulfilment of the Requirements for the Degree of Doctor of Philosophy

May 2024

FS 2024 17

© COPYRIGHT UPM

All material contained within the thesis, including without limitation text, logos, icons, photographs and all other artwork, is copyrighted material of Universiti Putra Malaysia unless otherwise stated. Use may be made of any material contained within the thesis for non-commercial purposes from the copyright holder. Commercial use of material may only be made with the express, prior, written permission of Universiti Putra Malaysia.

Copyright © Universiti Putra Malaysia

© COPYRIGHT UPM

Abstract of thesis presented to the Senate of Universiti Putra Malaysia in fulfilment of the requirement for the degree of Doctor of Philosophy

THERMAL FLUCTUATION AND EXCESS CONDUCTIVITY PROPERTIES FOR YBCO-ADDED CHITOSAN, CaO AND Ca COMPOUND

By

YAP SIEW HONG

May 2024

Chair : Mohd Mustafa bin Awang Kechik, PhD

Faculty : Science

Recently, significant progress has been made in developing high-quality bulk superconductors using rare earth materials, particularly $YBa_2Cu_3O_{7-\delta}$ (YBCO / Y-123), for potential applications. However, these materials often face the challenge of weak link behavior due to defects such as structural inconsistencies, pores, voids, and non-superconducting phases at the grain boundaries, leading to low critical current density (J_c). This project aims to understand the complex interactions among inhomogeneities, non-superconducting phases, and thermodynamic fluctuations of superconducting parameters during the superconducting transitions. The research involves incorporating various low concentrations (0.0100 wt.% $\leq x \leq$ 0.6000 wt.%) of chitosan (CHI), CaO and calcium compounds (CaO, $CaCO_3$, and $Ca(OH)_2$) extracted from chicken eggshells (CaES) into the YBCO matrix through thermal treatment method annealed under oxygen atmosphere and ambient. XRD results showed that all specimens crystallised into orthorhombic, Y-123 and non-superconducting phases such as Y-211 and $BaCuO_2$. These additions introduced

© COPYRIGHT UPM

different trends in grain degradation, spiral growth and nano entities within the YBCO matrix system. Investigations into the excess conductivity through DC resistivity measurements of these bulk granular specimens revealed a complete reduction in inter-layer coupling while preserving oxygen content and grain size. Furthermore, superconducting transition temperatures ($T_{c\text{-onset}}$, $T_{c\text{-offset}}$), superconducting transition width (ΔT_c) and inter-granular current density ($J_{c(0)}$) experienced significant improvements at deficient concentrations (0.0100 wt.%, 0.0375 wt.% and 0.0750 wt.%). The $J_{c(0)}$ reached peak value at 1.10×10^7 A/m^2 for specimen 0.0375 wt.% with CaO addition, which annealed in oxygen atmosphere, 1.03×10^7 A/m^2 for specimen 0.0375 wt.% with CHI addition annealed in ambient, and 9.41×10^6 A/m^2 for specimen 0.0100 wt.% with CaES addition annealed in ambient. The excess conductivity of these granular specimens revealed a dimensional crossover from 2D to 3D fluctuation as the temperature decreased. This could be attributed to the presence of non-superconducting phases (Y-211 and $BaCuO_2$) exhibiting inhomogeneity, which functioned as low-resistance grain boundaries and led to an improvement of thermal fluctuation parameters. It also serves as an effective superconducting connection between the grains. Incorporation below 0.0375 wt.% proved suitable for achieving finely scaled lattice defects that can act as effective pinning centres, dominating the 3D regime of thermal fluctuation, reducing flux motion and improving $J_{c(0)}$. This project underlines the potential of a sustainable approach involving incorporating low-concentration organic polymer (CHI), CaO and Ca compound.

Keywords: Critical current density, excess conductivity, intra-granular, superconducting parameters, thermal fluctuation

SDG: GOAL 7: Affordable and clean energy, GOAL 11: Sustainable Cities and Communities

© COPYRIGHT UPM

Abstrak tesis yang dikemukakan kepada Senat Universiti Putra Malaysia sebagai memenuhi keperluan untuk ijazah Doktor Falsafah

FLUKTUASI TERMAL DAN SIFAT-SIFAT KEKONDUKSIAN BERLEBIHAN BAGI YBCO DITAMBAH CHITOSAN, CaO DAN Ca KOMPAUN

Oleh

YAP SIEW HONG

Mei 2024

Pengerusi : Mohd Mustafa bin Awang Kechik, PhD
Fakulti : Sains

Baru-baru ini, kemajuan ketara telah dicapai dalam pembangunan superkonduktor pukal berkualiti tinggi menggunakan bahan nadir bumi, khususnya $YBa_2Cu_3O_{7-\delta}$ (YBCO / Y-123), untuk aplikasi yang berpotensi. Namun, bahan-bahan ini sering menghadapi cabaran kelakuan pautan lemah akibat kecacatan seperti ketidakkonsistenan struktur, liang-liang, lompang, dan fasa bukan superkonduktor pada sempadan butiran, yang membawa kepada ketumpatan arus kritikal (J_c) yang rendah. Projek ini bertujuan untuk memahami interaksi kompleks antara ketidakseragaman, fasa bukan superkonduktor, dan fluktuasi termodinamik parameter superkonduktor semasa peralihan superkonduktor. Penyelidikan ini melibatkan penggabungan pelbagai kepekatan rendah (0.0100 wt.% $\leq x \leq 0.6000$ wt.%) kitosan (CHI), CaO dan sebatian kalsium (CaO, $CaCO_3$, dan $Ca(OH)_2$) yang diekstrak dari kulit telur ayam (CaES) ke dalam matriks YBCO melalui kaedah rawatan haba yang disepuh di bawah atmosfera oksigen dan persekitaran. Keputusan XRD menunjukkan bahawa semua spesimen mengkristal menjadi ortorombik, Y-123 dan fasa bukan

© COPYRIGHT UPM

superkonduktor seperti Y-211 dan $BaCuO_2$. Penambahan ini memperkenalkan pelbagai trend dalam degradasi butiran, pertumbuhan spiral dan entiti nano dalam sistem matriks YBCO. Kajian mengenai konduktiviti lebihan melalui pengukuran rintangan DC pada spesimen granular pukal ini mendedahkan pengurangan sepenuhnya dalam penyambungan antara lapisan sambil mengekalkan kandungan oksigen dan saiz butiran. Selain itu, suhu peralihan superkonduktor ($T_{c\text{-onset}}$, $T_{c\text{-offset}}$), lebar peralihan superkonduktor (ΔT_c) dan ketumpatan arus antara butiran ($J_{c(0)}$) mengalami peningkatan ketara pada kepekatan rendah (0.0100 wt.%, 0.0375 wt.% dan 0.0750 wt.%). $J_{c(0)}$ mencapai nilai puncak pada 1.10×10^7 A/m^2 untuk spesimen 0.0375 wt.% dengan penambahan CaO, yang disepuh dalam atmosfera oksigen, 1.03×10^7 A/m^2 untuk spesimen 0.0375 wt.% dengan penambahan CHI yang disepuh dalam persekitaran, dan 9.41×10^6 A/m^2 untuk spesimen 0.0100 wt.% dengan penambahan CaES yang disepuh dalam persekitaran. Konduktiviti lebihan spesimen granular ini mendedahkan perubahan dimensi dari fluktuasi 2D ke 3D apabila suhu menurun. Ini boleh dikaitkan dengan kehadiran fasa bukan superkonduktor yang menunjukkan ketidakseragaman, yang berfungsi sebagai sempadan butiran rintangan rendah dan membawa kepada peningkatan parameter fluktuasi termal. Ia juga berfungsi sebagai sambungan superkonduktor yang efektif antara butiran. Penggabungan di bawah 0.0375 wt.% terbukti sesuai untuk mencapai kecacatan kekisi berskala halus yang boleh bertindak sebagai pusat pinning yang efektif, mendominasi rejim 3D fluktuasi termal, mengurangkan pergerakan fluks dan meningkatkan $J_{c(0)}$. Projek ini menekankan potensi pendekatan lestari yang melibatkan penggabungan polimer organik kepekatan rendah (CHI), CaO dan sebatian kalsium.

Kata Kunci: Fluktuasi termal, dalam butiran, kekonduksian berlebihan, ketumpatan arus kritikal, parameter superkonduktor

© COPYRIGHT UPM

SDG: MATLAMAT 7: Tenaga yang Mampu Milik dan Bersih, MATLAMAT 11: Bandar dan Komuniti Mampan

© COPYRIGHT UPM

ACKNOWLEDGEMENTS

I extend my gratitude and thanks to God for showering me with blessings beyond what I deserve, granting me the strength, peace of mind, and good health to complete this research successfully.

First and foremost, I extend my sincere gratitude to Assoc. Prof. Dr. Mohd. Mustafa bin Awang Kechik, who expertly guided me throughout my PhD journey. His professional support, patience, and extensive knowledge consistently kept me motivated and immersed in my research. Additionally, I would like to express my special thanks to my co-supervisor, Prof. Dr. Abdul Halim Shaari, and Assoc. Prof. Dr. Chen Soo Kien. I am also grateful to Assoc. Prof. Dr. Lim Kean Pah, Ts. Dr. Muhammad Kashfi Bin Shabdin, and Prof. Dr. Muralidhar Miryala (SIT), thank you for sharing your knowledge and expertise in this study.

I extend my gratitude to the Superconductors Thin Films and Laboratory teams members who, throughout my PhD journey, consistently encouraged me, moments of joy, and necessary diversions from the challenges of my research. Their support, through shared laughter, smiles, and words of encouragement, made the journey even more meaningful. I also want to acknowledge the Faculty of Science at UPM and thank everyone, particularly our lab assistant, Pn. Wan Nor Najwa, for their invaluable assistance and contributions. A special note of appreciation goes to Dr. Loh Zhi Wei, Dr. Mohd Hafiz Mohd Zaid and Dr. Khairul Khaizi Mohd Shariff for their provision of chemicals, including Ca compounds from chicken eggshells and chitosan derived from marine waste. Additionally, I am grateful to all the members of the UPM

© COPYRIGHT UPM

laboratory for their direct and indirect contributions, as their collective efforts played a significant role in assisting me during this research study.

I express profound gratitude to my parents and siblings, who supported me during challenging times, offering invaluable moral and emotional strength. My special loving thanks go to my husband, my daughter, and my sons, who have consistently been the driving and inspiring force behind me. I am also thankful to my in-laws' family for their unwavering support during my Ph.D. program. Pursuing it would have been impossible without their encouragement and support.

I extend my gratitude to everyone who has been a part of my PhD journey. A special acknowledgement goes to the Special Graduate Research Allowance Scheme for providing financial support throughout my studies. Lastly, but equally significantly, I appreciate all my colleagues and fellow students at UPM.

© COPYRIGHT UPM

This thesis was submitted to the Senate of Universiti Putra Malaysia and has been accepted as fulfilment of the requirement for the degree of Doctor of Philosophy. The members of the Supervisory Committee were as follows:

Mohd Mustafa bin Awang Kechik, PhD
Associate Professor
Faculty of Science
Universiti Putra Malaysia
(Chairman)

Halim Shaari, PhD
Professor
Faculty of Science
Universiti Putra Malaysia
(Member)

Chen Soo Kien, PhD
Professor
Faculty of Science
Universiti Putra Malaysia
(Member)

ZALILAH MOHD SHARIFF, PhD
Professor and Dean
School of Graduate Studies
Universiti Putra Malaysia

Date: 12 September 2024

© COPYRIGHT UPM

TABLE OF CONTENTS

		Page
ABSTRACT		i
ABSTRAK		iii
ACKNOWLEDGEMENTS		vi
APPROVAL		viii
DECLARATION		x
LIST OF TABLES		xv
LIST OF FIGURES		xix
LIST OF ABBREVIATIONS		xxvii
CHAPTER		
1	**INTRODUCTION**	1
	1.1 Basic Phenomena of Superconductors	1
	1.2 Types of Superconductors	4
	1.2.1 Type I Superconductors	4
	1.2.2 Type II Superconductors	5
	1.2.3 High-Temperature Superconductors (HTS)	6
	1.3 Research Innovation	7
	1.4 Problem Statement	8
	1.5 Objectives of Research	9
	1.6 Motivation for Incorporating Chitosan (Waste Marine Extraction), CaO, and Ca Compounds (Chicken Eggshells Extraction) into YBCO System	10
	1.7 Research Impact on Society, Economy and Nation	12
	1.8 Potential Applications for High-Temperature Superconductors	13
	1.9 Thesis Outlook and Overview	15
2	**LITERATURE REVIEW**	17
	2.1 Synthesis Methods of High Temperature Superconductors	17
	2.2 Thermal Treatment Method	18
	2.3 Inclusion of Chitosan in YBCO	20
	2.4 Inclusion of Calcium in YBCO	22
	2.5 The Pseudogap Phenomena in High-Temperature Superconductors	29
	2.6 Thermal Fluctuation and Excess Conductivity Study of YBCO	32
3	**THEORY OF SUPERCONDUCTORS**	44
	3.1 The Bardeen, Cooper, and Schrieffer (BCS) Theory	44
	3.2 General Properties of Granular Superconductors	45
	3.3 Crystal Structure of $REBa_2Cu_3O_{7-\delta}$ / $YBa_2Cu_3O_{7-\delta}$	47
	3.4 Pinning Engineering	49

© COPYRIGHT UPM

3.4.1 Pining Centre and Role of Defects 50
3.4.2 Defects' Role in Pinning Vortices 54
3.5 Normal State and Paracoherent Resistivity 55
3.6 Excess Conductivity Study 59
3.6.1 Almalazov Larkin Approach 61
3.6.2 Lawrence-Doniach Approach 63
3.6.3 The Dimensionality of Thermal Fluctuation - Gaussian Fluctuation 66
3.6.4 Fluctuation Regimes in YBCO: Critical Fluctuation 66
3.6.5 Fluctuation Regimes in YBCO: 1D Fluctuation 67
3.6.6 Fluctuation Regimes in YBCO: Shortwave Fluctuation 67
3.6.7 Estimation of Critical Current Density, $J_{c(0)}$ from The Excess Conductivity Analysis 68

4 MATERIALS AND METHODS 70
4.1 Sample Preparation Using Thermal Treatment Method 70
4.1.1 Primary Chemicals 72
4.1.2 Solutions Mixing Process 73
4.1.3 Drying Process 74
4.1.4 Pre-calcination Process 75
4.1.5 Calcination Process 76
4.1.6 Pelletising, Sintering and Annealing Process 77
4.2 Sample Characterizations Technique 79
4.2.1 Thermogravimetric Analysis (TGA) 80
4.2.2 X-ray Diffraction (XRD) 82
4.2.3 Field Emission Scanning Electron Microscopy (FESEM) 84
4.2.4 Energy Dispersion X-ray (EDX) 86
4.2.5 DC Resistivity Measurement (R-T) 87

5 RESULTS AND DISCUSSION 91
5.1 YBCO Added Chitosan (Extraction Waste-Marine) / (YBCO-CHI) Annealed in Oxygen Flow and Ambient Conditions (Part 1) 92
5.1.1 TGA Analysis for Pure YBCO and Pure Chitosan (CHI) 92
5.1.2 XRD Analysis-Phase Formation 96
5.1.3 FESEM and EDX Analysis-Microstructural Formation 103
5.1.4 Resistivity Measurement Analysis – Electrical Transport Properties 118
5.1.5 Dimensionality of Fluctuation Study 126
5.1.6 Excess Conductivity Properties – Critical Current Density, $J_{c(0)}$ 129
5.1.7 Summary for Synthesis of YBCO-CHI 134

© COPYRIGHT UPM

5.2 YBCO Added CaO Commercial / (YBCO-CaO) Annealed in Oxygen Flow and Ambient Conditions (Part 2) 137
5.2.1 TGA Analysis for Pure YBCO and CaO Commercial 137
5.2.2 XRD Analysis-Phase Formation 139
5.2.3 FESEM and EDX Analysis-Microstructural Formation 145
5.2.4 Resistivity Measurement Analysis – Electrical Transport Properties 157
5.2.5 Dimensionality of Fluctuation Study 167
5.2.6 Excess Conductivity Properties – Critical Current Density, $J_{c(0)}$ 170
5.2.7 Summary for Synthesis of YBCO-CaO 176
5.3 YBCO Added Ca Compounds (Extraction Chicken Eggshells) / (YBCO-CaES) Annealed in Oxygen Flow and Ambient Conditions (Part 3) 178
5.3.1 TGA Analysis for Pure YBCO and Ca Compounds (CaES) 179
5.3.2 XRD Analysis-Phase Formation 180
5.3.3 FESEM and EDX Analysis-Microstructural Formation 187
5.3.4 Resistivity Measurement Analysis – Electrical Transport Properties 200
5.3.5 Dimensionality of Fluctuation Study 208
5.3.6 Excess Conductivity Properties – Critical Current Density, $J_{c(0)}$ 211
5.3.7 Summary for Synthesis of YBCO-CaES 216
5.4 The Comparison between YBCO-CaO and YBCO-CaES System 218
5.5 The Comparison of The Excess Conductivity Properties for All Specimens 220
5.6 Summary of Research 224

6 CONCLUSION AND RECOMMENDATIONS FOR FUTURE RESEARCH 230
6.1 Conclusion of The Research Work and Important Findings 230
6.2 The Contribution of Research Findings to The Community Society 234
6.3 Recommendation for Future Works 235

REFERENCES 238
APPENDICES 256
BIODATA OF STUDENT 273
LIST OF PUBLICATIONS 274

© COPYRIGHT UPM

LIST OF TABLES

Table		Page
2.1	Advantages and disadvantages of thermal treatment method	19
2.2	The important superconducting parameters derived from the analysis of excess conductivity	40
4.1	Chemical inventory and corresponding specifications	73
4.2	The quantity of chemical substances employed in the formulation of a 10 g mixture of YBCO powder	73
5.1	Summary of decomposition details for pure YBCO and pure CHI	95
5.2	The lattice parameters, orthorhombicity, and oxygen content for YBCO-CHI at different concentrations, annealed in oxygen flow	101
5.3	The lattice parameters, orthorhombicity and oxygen content for YBCO-CHI at different concentrations, annealed in ambient	102
5.4	The volume fractions, the volume of unit cell Y-123, FWHM, crystallite size and lattice strain for the YBCO-CHI at different concentrations, annealed in oxygen flow	102
5.5	The volume fractions, the volume of unit cell Y-123, FWHM, crystallite size and lattice strain for the YBCO-CHI at different concentrations, annealed in ambient	102
5.6	Average grain sizes for all specimens YBCO-CHI, annealed in oxygen flow	106
5.7	Average grain sizes for all specimens YBCO-CHI, annealed in ambient	108
5.8	The atomic % of elements present in the pure CHI scan at two different regions	112
5.9	The atomic % of elements contain scan by area for YBCO-CHI 0.0000 wt.%, 0.0100 wt.% and 0.6000 wt.%, annealed in oxygen flow	115
5.10	The atomic % of elements contain scan by area in YBCO-CHI 0.0000 wt.%, 0.0100 wt.% and 0.6000 wt.% annealed in ambient	117

© COPYRIGHT UPM

5.11	The superconducting parameters for YBCO-CHI at different concentrations, annealed in oxygen flow	125
5.12	The superconducting parameters for YBCO-CHI at different concentrations, annealed in ambient	125
5.13	Superconducting parameters extracted from excess conductivity analysis for YBCO-CHI at different concentrations, annealed in oxygen flow	132
5.14	Superconducting parameters extracted from excess conductivity analysis for YBCO-CHI at different concentrations, annealed in ambient	133
5.15	Summary of decomposition details for pure YBCO and pure CaO	139
5.16	The lattice parameters, orthorhombicity and oxygen content for YBCO-CaO at different concentrations, annealed in oxygen flow	144
5.17	The lattice parameters, orthorhombicity and oxygen content for YBCO-CaO at different concentrations, annealed in ambient	144
5.18	The volume fractions, the volume of unit cell Y-123, FWHM, crystallite size and lattice strain for YBCO-CaO at different concentrations, annealed in oxygen flow	144
5.19	The volume fractions, the volume of unit cell Y-123, FWHM, crystallite size and lattice strain for the YBCO-CaO at different concentrations, annealed in ambient	145
5.20	Average grain sizes for all specimens YBCO-CaO at difference concentrations, annealed in oxygen flow	148
5.21	Average grain sizes for all specimens YBCO-CaO at different concentrations, annealed in ambient	150
5.22	The atomic % of elements present and the atomic ratio for pure CaO, as well as YBCO-CaO at concentration of 0.6000, annealed in oxygen flow	155
5.23	The atomic % of elements present and the atomic ratio for pure YBCO, as well as YBCO-CaO at concentration, 0.0100 wt.% (with EDX mapping), 0.0075 wt.% (with EDX mapping), annealed in ambient	157
5.24	The superconducting parameters for YBCO-CaO at different concentrations, annealed in oxygen flow	166

© COPYRIGHT UPM

5.25	The superconducting parameters for YBCO-CaO at different concentrations, annealed in ambient	166
5.26	Superconducting parameters extracted from excess conductivity analysis for YBCO-CaO at different concentrations, annealed in oxygen flow	173
5.27	Superconducting parameters extracted from excess conductivity analysis for YBCO-CaO at different concentrations, annealed in ambient	174
5.28	Summary of decomposition details for pure YBCO and pure CaES	180
5.29	The lattice parameters, orthorhombicity and oxygen content for YBCO-CaES at different concentrations, annealed in oxygen flow	185
5.30	The lattice parameters, orthorhombicity, and oxygen content of YBCO-CaES at different concentrations, annealed in ambient	185
5.31	The volume fractions, the volume of unit cell Y-123, FWHM, crystallite size and lattice strain for the YBCO-CaES at different concentrations, annealed in oxygen flow	186
5.32	The volume fractions, unit cell volume of Y-123, full width at half maximum (FWHM), crystallite size, and lattice strain of YBCO-CaES at different concentrations, annealed in ambient	186
5.33	Average grain sizes for all specimens YBCO-CaES at different concentrations, annealed in oxygen atmosphere	189
5.34	Average grain sizes for all specimens YBCO-CaES at different concentrations, annealed in ambient	191
5.35	The atomic % of elements present and the atomic ratio for pure CaES, YBCO-CaES at concentrations of 0.0375 wt.% (EDX mapping), 0.0075 wt.%, 0.1500 wt.%, and 0.3000 wt.%, annealed in oxygen flow	197
5.36	The atomic % of pure YBCO, as well as YBCO-CaES at concentrations of 0.0375 wt.% (as depicted in EDX mapping), 0.0075 wt.%, 0.1500 wt.%, 0.3000 wt.%, and 0.6000 wt.%, annealed in ambient	200
5.37	The superconducting parameters for YBCO-CaES at different concentrations, annealed in oxygen flow	207
5.38	The superconducting parameters for YBCO-CaES at different	207

© COPYRIGHT UPM

concentrations, annealed in ambient

5.39 Superconducting parameters extracted from excess conductivity analysis for YBCO-CaES at different concentrations, annealed in oxygen flow 213

5.40 Superconducting parameters from excess conductivity analysis for YBCO-CaES at different concentrations, annealed in ambient 214

5.41 The comparison of all important physical properties from characterization results for YBCO-CaO and YBCO-CaES system 220

© COPYRIGHT UPM

LIST OF FIGURES

Figure		Page
1.1	The temperature-dependent behaviour of mercury's resistance illustrates its gradual disappearance as it transitions into a superconducting state	2
1.2	Depicting the manifestation of perfect diamagnetism in superconductors	3
1.3	The relationship between the internal magnetic field of the material and the external magnetic field for type I superconductor	5
1.4	The relationship between the internal magnetic field of the material and the external magnetic field for type II superconductor	6
1.5	The potential technological applications of High-Temperature Superconductors	15
2.1	The visual representation depicts the proposed mechanism of interaction between PVP and metallic ions	20
2.2	The temperature dependency of critical current densities (J_c) at grain boundaries exhibits notable enhancement across various doping configurations, suggesting a significant improvement in J_c within doping heterostructures	27
2.3	Phase diagram for cuprate superconductors illustrating the relationship between hole concentration (doping), *p*. T^* stands notably higher than T_N, approximately $T^* \approx 2\ T_N$	30
2.4	SEM images depicting Y-123 nanoparticles on the specimens (a) Pure Y-123 and (b) B-milled Y-123 added $AgNO_3$	38
3.1	Illustration depicting the formation of Cooper pairs	45
3.2	Illustration depicting the atomic arrangement within a grain and at the grain boundary in a polycrystalline material, where the periodic three-dimensional atomic structure encounters a boundary between grains possessing different crystal orientations	46
3.3	A broad overview of a polycrystalline sample showcases the currents between grains (inter-grain current) within a single grain (intra-grain current), and the coupling that occurs	47

© COPYRIGHT UPM

between neighbouring grains (inter-grain coupling)

3.4	(a) Crystal structure of REBCO exemplified by $YBa_2Cu_3O_{y-\delta}$ (YBCO / Y-123); (b) Single perovskite structure ABO_3; (c) Double perovskite structure $A_2BB'O_6$	49
3.5	Illustrations of the dimensionality for various types of pinning centers and examples of typical defects for each case.	53
3.6	A visual depiction illustrating the penetration of a magnetic field into a superconductor in clustered bundles	55
3.7	Schematic figure showing typical resistivity vs temperature curve for a granular superconductor (YBCO)	59
3.8	ln-ln plot of excess conductivity as a function of reduced temperature	65
4.1	Flowchart of synthesising and characterising of all specimens, YBCO added CHI, CaO commercial and CaES	72
4.2	The blend of the metal nitrate employed and a 300 ml aqueous solution containing 2% PVP underwent stirring for 2 hours at 80 °C, utilising a magnetic stirrer set at 850 rpm	74
4.3	(a) The light green-blue mixture in the petri dish that is ready for drying; (b) The dried green gel post-drying process	75
4.4	(a) The green fine powder after grinded with mortar and pestle; (b) The crucible was inserted into the box furnace	75
4.5	The specified temperature-time schedule designed for the pre-calcination process	76
4.6	The light-grey powder obtained after the pre-calcination process	77
4.7	The designated temperature-time schedule crafted for the calcination process	77
4.8	The pelletised specimens were shaped into a circular form	78
4.9	The specified temperature-time schedule devised for both the sintering and annealing processes	79
4.10	The setup involves the sintering process coupled with annealing using a double-tube furnace	79
4.11	Schematic diagram of the working principle of a	80

© COPYRIGHT UPM

	thermogravimetric analyser	
4.12	Schematic diagram of Mettler Toledo TGA/DSC 1	82
4.13	Scattered X-rays by a crystal lattice	83
4.14	Schematic diagram of FESEM working principle	86
4.15	A diagram illustrating the measurement of the averaged grain size for a specific individual grain	86
4.16	A visual representation illustrating the underlying principle of EDX	87
4.17	Illustration showing the configuration of the four-point probes setup used for resistivity measurement	90
4.18	Within the four-probe setup, the current circulates through the first and fourth probes while measuring the voltage difference between the second and third inner probes	90
5.1	TGA-DTA analysis for pure YBCO	94
5.2	TGA-DTA analysis for pure chitosan (CHI)	95
5.3	XRD pattern of YBCO-CHI with various concentrations, annealed in oxygen flow	97
5.4	XRD pattern of YBCO-CHI at different concentrations, annealed in ambient	97
5.5	XRD pattern of pure CHI	98
5.6	FESEM surface micrographs for YBC-CHI at different concentrations, (a) 0.0000 wt.%, (b) 0.0100 wt.%, (c) 0.0375 wt.%, (d) 0.0750 wt.%, (e) 0.1500 wt.%, (f) 0.3000 wt.% and (g) 0.6000 wt.%), annealed in oxygen flow	105
5.7	FESEM surface micrographs for YBC-CHI at different concentrations, (a) 0.0000 wt.%, (b) 0.0100 wt.%, (c) 0.0375 wt.%, (d) 0.0750 wt.%, (e) 0.1500 wt.%, (f) 0.3000 wt.% and (g) 0.6000 wt.%), annealed in ambient	107
5.8	High magnification FESEM images for YBCO-CHI at different concentrations, (a) 0.0000 wt.%, (b) 0.0100 wt.%, (c) 0.0375 wt.%, (d) 0.0750 wt.%, (e) 0.1500 wt.%, (f) 0.3000 wt.% and (g) 0.6000 wt.%, annealed in oxygen flow	110
5.9	High magnification FESEM images for YBCO-CHI at	111

© COPYRIGHT UPM

different concentrations, (a) 0.0000 wt.%, (b) 0.0100 wt.%, (c) 0.0375 wt.%, (d) 0.0750 wt.%, (e) 0.1500 wt.%, (f) 0.3000 wt.% and (g) 0.6000 wt.%, annealed in ambient

5.10 EDX elemental spectra for pure CHI scan at two different regions (a) spectrum 1 and (b) spectrum 2 112

5.11 EDX elemental analysis for (a) pure YBCO, (b) YBCO -CHI 0.0100 wt.% (EDX mapping) and (c) 0.6000 wt.% (EDX mapping), annealed in oxygen flow 114

5.12 EDX elemental analysis for (a) pure YBCO, (b) YBCO -CHI 0.0100 wt.% (EDX mapping) and (c) 0.6000 wt.% (EDX mapping), annealed in ambient 117

5.13 (a) Plot of normalised resistivity, $\rho(T)$, against the temperature range of 30 to 300 K, and (b) a close-up view of the temperature ranges from 84 K to 96 K for YBCO-CHI at different concentrations, annealed in oxygen flow 119

5.14 (a) Plot of normalised resistivity, $\rho(T)$, against the temperature range of 30 to 300 K, and (b) a close-up view of the temperature ranges from 86 K to 96 K for YBCO-CHI with different concentrations, annealed in ambient 120

5.15 Analysis of the derivative resistivity (a) in the temperature range of 30 to 300 K, and (b) a close-up examination within the range of 86 to 96 K for the YBCO-CHI at different concentrations, annealed in oxygen flow 121

5.16 Analysis of the derivative resistivity (a) in the temperature range of 30 to 300 K, and (b) a close-up examination within the range of 86 to 96 K for the YBCO-CHI at different concentrations, annealed in ambient 122

5.17 Logarithmic plots of excess conductivity, $\Delta\sigma$ as a function of the reduced temperature, ε for YBCO-CHI at different concentrations, from 0.0100 wt.% to 0.6000 wt.% annealed in oxygen flow 128

5.18 Logarithmic plots of excess conductivity, $\Delta\sigma$ as a function of the reduced temperature, ε for YBCO-CHI at different concentrations, from 0.0100 wt.% to 0.6000 wt.% annealed in ambient 129

5.19 Evolutions of the $J_{c(0)}$ and $\xi_{c(0)}$ for YBCO-CHI at different concentrations, annealed in oxygen flow 133

5.20 Evolutions of the $J_{c(0)}$ and $\xi_{c(0)}$ for YBCO-CHI at different concentrations, annealed in ambient 134

© COPYRIGHT UPM

5.21	TGA and DTA analysis for CaO Commercial	138
5.22	XRD pattern of YBCO-CaO at different concentrations, annealed in oxygen flow	140
5.23	XRD pattern of YBCO-CaO at different concentrations, annealed in ambient	140
5.24	XRD pattern of CaO Commercial	141
5.25	FESEM surface micrographs for YBCO-CaO at different concentrations (a) 0.0000 wt.%, (b) 0.0100 wt.%, (c) 0.0375 wt.%, (d) 0.0750 wt.%, (e) 0.1500 wt.%, (f) 0.3000 wt.% and (g) 0.6000 wt.%, annealed in oxygen flow	148
5.26	FESEM surface micrographs for YBCO-CaO at different concentrations, (a) 0.0000 wt.%, (b) 0.0100 wt.%, (c) 0.0375 wt.%, (d) 0.0750 wt.%, (e) 0.1500 wt.%, (f) 0.3000 wt.% and (g) 0.6000 wt.%, annealed in ambient	150
5.27	High magnification FESEM images for YBCO-CaO at different concentrations, (a) 0.0000 wt.%, (b) 0.0100 wt.%, (c) 0.0375 wt.%, (d) 0.0750 wt.%, (e) 0.1500 wt.%, (f) 0.3000 wt.% and (g) 0.6000 wt.%, annealed in oxygen flow	152
5.28	High magnification FESEM images for YBCO-CaO at different concentrations, (a) 0.0000 wt.%, (b) 0.0100 wt.%, (c) 0.0375 wt.%, (d) 0.0750 wt.%, (e) 0.1500 wt.%, (f) 0.3000 wt.% and (g) 0.6000 wt.%, annealed in ambient	153
5.29	EDX elemental analysis for (a) pure CaO, (b) Pure YBCO and (c) YBCO-CaO 0.6000 wt.% (low magnification 600 □), annealed in oxygen flow	155
5.30	EDX elemental analysis for (a) Pure YBCO and YBCO-CaO at concentrations, (b) 0.0100 wt.% (EDX mapping), (c) 0.0750 wt.%, annealed in ambient	157
5.31	**(**a) Plot of normalised resistivity, $\rho(T)$, against the temperature range of 30 to 300 K, and (b) a close-up view of the temperature ranges from 82 K to 96 K for YBCO-CaO at different concentrations, annealed in oxygen flow	159
5.32	(a) Plot of normalised resistivity, $\rho(T)$, against the temperature range of 30 to 300 K, and (b) a close-up view of the temperature ranges from 82 K to 96 K for YBCO-CaO at different concentrations, annealed in ambient	160
5.33	Analysis of the derivative resistivity (a) in the temperature range of 30 to 300 K, and (b) a close-up examination within	162

© COPYRIGHT UPM

	the range of 82 to 96 K for the YBCO-CaO at different concentrations, annealed in oxygen flow	
5.34	Analysis of the derivative resistivity (a) in the temperature range of 30 to 300 K, and (b) a close-up examination within the range of 82 to 96 K for the YBCO-CaO at different concentrations, annealed in ambient	163
5.35	Logarithmic plots of excess conductivity, $\Delta\sigma$ as a function of the reduced temperature, ε for YBCO-CaO at different concentrations, annealed in oxygen flow	168
5.36	Logarithmic plots of excess conductivity, $\Delta\sigma$ as a function of the reduced temperature, ε for YBCO-CaO at different concentrations, annealed in ambient	169
5.37	Evolutions of the $J_{c(0)}$ and $\xi_{c(0)}$ for YBCO-CaO at different concentrations, annealed in oxygen flow	176
5.38	Evolutions of the $J_{c(0)}$ and $\xi_{c(0)}$ for YBCO-CaO at different concentrations, annealed in ambient	176
5.39	TGA and DTA analysis for Ca compounds extracted from chicken eggshells (CaES)	179
5.40	XRD pattern of YBCO added with CaES at different concentrations, annealed in oxygen flow	181
5.41	XRD pattern of YBCO-CaES at different concentrations, annealed in ambient	182
5.42	XRD pattern of pure CaES subjected to calcination at 900 °C for 2 hours	182
5.43	FESEM surface micrographs for YBCO-CaES at different concentrations, (a) 0.0000 wt.%, (b) 0.0100 wt.%, (c) 0.0375 wt.%, (d) 0.0750 wt.%, (e) 0.1500 wt.%, (f) 0.3000 wt.% and (g) 0.6000 wt.%, annealed in oxygen flow	189
5.44	FESEM surface micrographs for YBCO-CaES at different concentrations, (a) 0.0000 wt.%, (b) 0.0100 wt.%, (c) 0.0375 wt.%, (d) 0.0750 wt.%, (e) 0.1500 wt.%, (f) 0.3000 wt.% and (g) 0.6000 wt.%, annealed in ambient	191
5.45	High magnification FESEM images for YBCO-CaES at different concentrations, (a) 0.0000 wt.%, (b) 0.0100 wt.%, (c) 0.0375 wt.%, (d) 0.0750 wt.%, (e) 0.1500 wt.%, (f) 0.3000 wt.% and (g) 0.6000 wt.%, annealed in oxygen flow	193
5.46	High magnification FESEM images for YBCO-CaES at different concentrations, (a) 0.0000 wt.%, (b) 0.0100 wt.%, (c)	194

© COPYRIGHT UPM

	0.0375 wt.%, (d) 0.0750 wt.%, (e) 0.1500 wt.%, (f) 0.3000 wt.% and (g) 0.6000 wt.%, annealed in ambient	
5.47	EDX elemental analysis for (a) pure CaES and YBCO-CaES at concentrations, (b) 0.0375 wt.% (EDX mapping), (c) 0.0750 wt.%, (d) 0.1500 wt.%, and (e) 0.3000 wt.%, annealed in oxygen flow	197
5.48	High magnification (100,000 ×) EDX spectra and image for YBCO-CaES 0.1500 wt.%, annealed in oxygen flow	198
5.49	EDX elemental analysis for (a) Pure YBCO and YBCO-CaES at concentrations, (b) 0.0375 wt.% (EDX mapping), (c) 0.0750 wt.%, (d) 0.1500 wt.%, and (e) 0.3000 wt.%, (f) 0.6000 wt.% annealed in ambient	199
5.50	(a) Plot of normalised resistivity, $\rho(T)$, against the temperature range of 30 to 300 K, and (b) a close-up view of the temperature ranges from 68 K to 98 K for YBCO-CaES at different concentrations, annealed in oxygen flow	202
5.51	(a) Plot of normalised resistivity, $\rho(T)$, against the temperature range of 30 to 300 K, and (b) a close-up view of the temperature range from 80 K to 96 K for YBCO-CaES at different concentrations, annealed in ambient	203
5.52	Analysis of the derivative resistivity (a) in the temperature range of 30 to 300 K, and (b) a close-up examination within the range of 68 to 98 K for the YBCO-CaES at different concentrations, annealed in oxygen flow	204
5.53	Analysis of the derivative resistivity (a) in the temperature range of 30 to 300 K, and (b) a close-up examination within the range of 80 to 98 K for the YBCO-CaES at different concentrations, annealed in ambient	205
5.54	Logarithmic plots of excess conductivity, $\Delta\sigma$ as a function of the reduced temperature, ε for YBCO-CaES at different concentrations, from 0.0100 wt.% to 0.6000 wt.%, annealed in oxygen flow	209
5.55	Logarithmic plots of excess conductivity, $\Delta\sigma$ as a function of the reduced temperature, ε for YBCO-CaES at different concentrations, from 0.0100 wt.% to 0.6000 wt.% annealed in ambient	210
5.56	Variations in the $J_{c(0)}$, and $\xi_{c(0)}$ in YBCO-CaES at different concentrations, annealed in an oxygen flow	215
5.57	Variations in the $J_{c(0)}$, and $\xi_{c(0)}$ in YBCO-CaES at different concentrations, annealed in ambient	216

© COPYRIGHT UPM

5.58	The comparison of $J_{c(0)}$ between six series of YBCO-CHI, YBCO-CaO, and YBCO-CaES annealed under both oxygen flow and ambient conditions	221
5.59	The comparison of high-magnification FESEM images (100,000 X) among distinct series of YBCO-CHI, YBCO-CaO, and YBCO-CaES focuses on the optimal specimens within each series, all annealed under both oxygen flow and ambient conditions	223

© COPYRIGHT UPM

LIST OF ABBREVIATIONS

A	Ampere
Å	Angstrom
a.u.	Arbitrary unit
APCs	Artificial pinning centers
AL	Aslamasov and Larkin
$BaCuO_2$	Barium Copper Oxide
REBCO	Bulk rare earth based high-temperature superconductors
Ca	Calcium
CaES	Ca Compounds extracted from chicken eggshells
CaO	Calcium oxide
CHI	Chitosan derived from marine waste
$\xi_c(0)$	Coherence length along the c-axis at zero temperature
J_c	Critical current density
$J_{c(0)}$	Critical current density at zero Kelvin
H_c	Critical magnetic field
T_c	Critical temperature
DTA	Derivative thermal analysis
d	Effective layer thickness of the 2D system
ρ	Electrical resistivity
EDX	Energy dispersive X-ray spectroscopy
σ	Excess conductivity
FESEM	Field emission scanning electron microscopy

© COPYRIGHT UPM

ϕ_o	Flux-quantum number
FWHM	Full width at half maximum
T_G	Ginzburg- Landau Temperature
HTS	High-temperature superconductors
p	Hole concentration
h	Hour
ICSD	Inorganic Crystal Structure Database
E_J	Josephson coupling
K	Kelvin
a, b, c	Lattice parameters
LD	Lawrence and Doniach
T_{LD}	Lawrence-Doniach crossover temperature
λ	London penetration depth
H_{c1}	Lower critical magnetic field
H_{c2}	Upper critical magnetic field
H	Magnetic Field
MT	Maki-Thompson
T_c^{MF}	Mean-field critical temperature
$\rho_n(T)$	Normal state resistivity
$T_{c\text{-onset}}$	Onset critical temperature
$T_{c\text{-offset}}$	Offset critical temperature
$O_{7-\delta}$	Oxygen content
ρ_p	Paracoherent resistivity

© COPYRIGHT UPM

λ	Penetration depth
$\lambda(0)$	Penetration depth at zero Kelvin
PVP	Polyvinyl pyrrolidone
T^*	Pseudogap temperature
ρ_o	Residual resistivity
T_{SW}	Short-Wave Fluctuation Temperature
SMES	Superconductors Magnetic energy storage
SCOPF	Superconducting order parameter fluctuations
ΔT_c	Superconducting transition width
TGA	Thermogravimetry Analysis
XRD	X-Ray Diffractometer
Y-123	$YBa_2Cu_3O_{7-\delta}$ / YBCO
Y-211	$Y_2BaCu_1O_5$

© COPYRIGHT UPM

CHAPTER 1

INTRODUCTION

This chapter introduces the fundamental aspects of superconductivity, elucidating some elementary theories associated with it. It further delineates the research's problem statement and objectives, delving into its innovative and commercial value. Additionally, it discusses the potential applications of high-temperature superconductors (HTS) materials and addresses global issues amid HTS technology development. This chapter concludes with a brief preview of the thesis and a summary of the research conducted in this project.

1.1 Basic Phenomena of Superconductors

Superconductivity refers to the complete absence of electrical resistance and the ability to repel magnetic fields in specific materials once they're cooled below a critical temperature. Dutch physicist Heike Kamerlingh Onnes unearthed this phenomenon in Leiden on April 8, 1911. Much like ferromagnetism and atomic spectral lines, superconductivity is a phenomenon rooted in quantum mechanics. His groundbreaking revelation was that as the mercury (Hg) temperature decreased, its resistance didn't decrease gradually; instead, it abruptly plummeted to zero at approximately 4.2 K (Owens et al., 2002; Van et al., 2010). Similar behaviour was observed in other elements like Pb, Sn, and Al, with critical temperatures ranging between 4 to 10 K. Figure 1.1 shows a plot of Onnes's original resistance measurements, the first

© COPYRIGHT UPM

observation of superconductivity. Resistance drops sharply over a very narrow temperature range, from 0.11 ohm at 4.22 K to 0.00001 ohm (10 - 5 ohm) at 4.19 K.

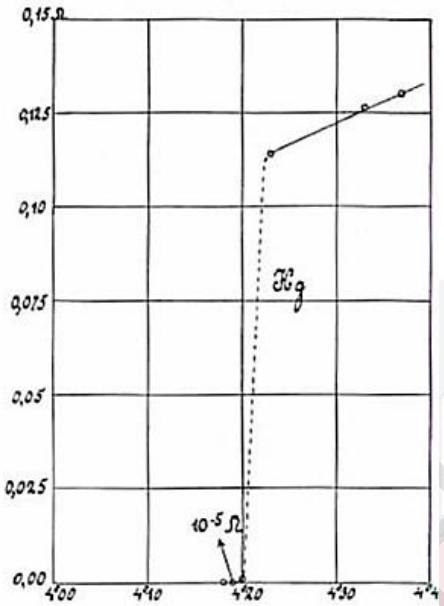

Figure 1.1: The temperature-dependent behaviour of mercury's resistance illustrates its gradual disappearance as it transitions into a superconducting state (Van et al., 2010)

Although Onnes received the Nobel Prize in 1913 for his achievement in helium liquefaction, his discovery of superconductivity needs to be specifically honored. The total repulsion of a magnetic field by a superconducting sample below its transition temperature (T_c) is termed the "Meissner effect," exhibiting perfect diamagnetism (Figure 1.2). The discovery of superconductors property was credited to Meissner and Ochsenfeld in 1933. The Meissner effect describes the complete expulsion of magnetic field lines from within a superconductor during its transition to the superconducting state. This effect signifies that superconductivity isn't just an ideal form of perfect conductivity in classical physics. While the electrical resistivity of a metallic conductor gradually decreases with lowering temperature, impurities and defects limit this decrease in materials like copper or silver. Even at temperatures near absolute zero,

© COPYRIGHT UPM

these normal conductors maintain some resistance. In contrast, resistance suddenly vanishes in a superconductor when the material is cooled below its critical temperature. In a superconducting loop, an electric current can flow continuously without the need for an external power source. Perfect diamagnetism observed in superconductors clearly indicates the true thermodynamic nature of superconductivity. When a material transitions from its normal to the superconducting state, it undergoes a significant thermodynamic phase transition. This shift marks a fundamental change in the material's behaviour and properties.

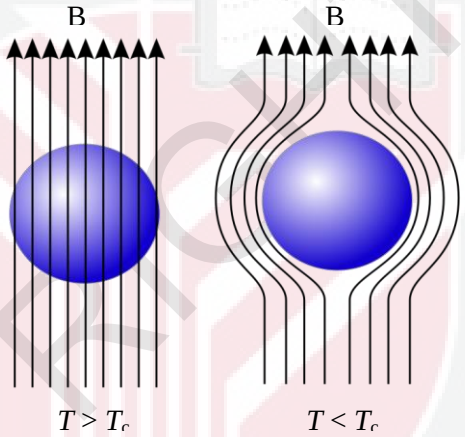

Figure 1.2: Depicting the manifestation of perfect diamagnetism in superconductors (Meissner effect, 2023)

In 1987, at the University of Houston, Paul Chu and his students discovered the first ceramic material with a transition temperature more significant than the boiling point of liquid nitrogen at 77 K, i.e. YBCO or Y-123. It was discovered that some cuprate-perovskite ceramic materials have a critical temperature above 90 K (- 183 °C). Such a high transition temperature is theoretically impossible for a conventional superconductor, leading the materials to be termed high-temperature superconductors.

© COPYRIGHT UPM

1.2 Types of Superconductors

Superconductors can be classified according to their reaction to an externally applied magnetic field, with categorisation dependent on their diamagnetic response:

(i) Type I Superconductors

(ii) Type II Superconductors

1.2.1 Type I Superconductors

Superconductors of type I, known as soft and pure superconductors, exhibit a rapid breakdown of their smaller magnetic fields, H values, even when exposed to relatively weak external magnetic fields. In type I superconductors, superconductivity undergoes an abrupt termination through a first-order phase transition when the intensity of the applied field exceeds a critical value, H_c (Owens et al., 2002). This type of superconductivity is commonly seen in pure metals like aluminium, lead, mercury, and others. Figure 1.3 demonstrates the correlation between the internal magnetic field within the material and the external field. In type I superconductors, the external magnetic field is kept out of the material until it reaches the critical field (H_c). Once this threshold is surpassed, the superconducting state is disrupted, enabling the complete penetration of the applied field into the material. Their transitions are sharply defined, with resistance plummeting to zero within a narrow temperature range, as depicted in the case of mercury in Figure 1.1. Due to their lower values of H_c and T_c, type I superconductors lack significant practical applications.

© COPYRIGHT UPM

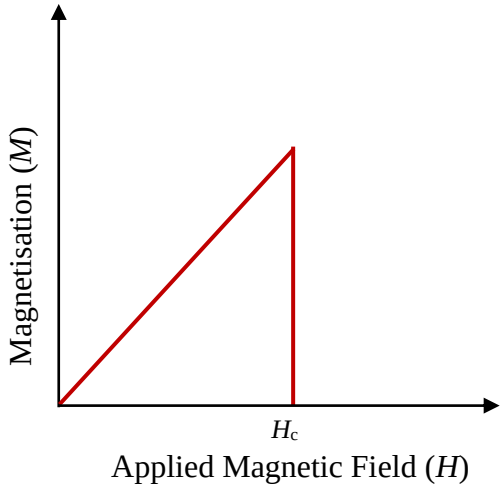

Figure 1.3: The relationship between the internal magnetic field of the material and the external magnetic field for type I superconductor (Owens et al., 2002)

1.2.2 Type II Superconductors

Since approximately 1962, there has been a widespread acknowledgement of a distinct category of superconductors known as type II superconductors (Goodman, 1966). They are distinguished by their display of a novel form of reversible magnetic behaviour. This revelation has provided insight into various superconducting properties of numerous elements and a wide array of previously ununderstood alloys. It is essential to highlight that type II encompasses all chemical compounds and alloys, whereas type I superconductivity excludes elements.

A type II superconductor is distinguished by the emergence of magnetic vortices when subjected to an applied magnetic field, occurring above a certain critical field strength, H_{c1} (Owens et al., 2002). The density of these vortices increases proportionally with the rising field strength. Superconductivity is entirely disrupted at a higher critical field, H_{c2}, as depicted in Figure 1.4. In this type, magnetic field penetration begins at a lower critical field, H_{c1}, and progresses with increasing applied field until reaching

© COPYRIGHT UPM

the upper critical field, H_{c2}, leading to the loss of the superconducting state across the entire material. In regions where the applied field is below H_{c1} and no flux penetrates, the material is in what is known as the Meissner state. Between the two critical fields, H_{c1} and H_{c2}, a mixed state exists with sections of non-superconducting (i.e., normal) material interspersed within a perfectly superconducting matrix. Below H_{c1}, type II behaves similarly to type I; above H_{c2}, it reverts to a normal state.

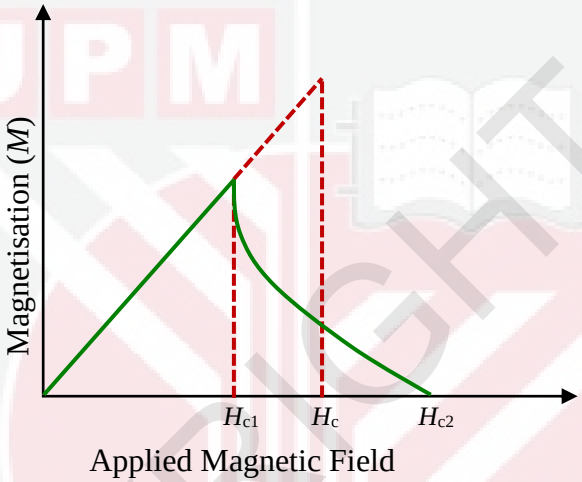

Figure 1.4: The relationship between the internal magnetic field of the material and the external magnetic field for type II superconductor (Owens et al., 2002)

1.2.3 High-temperature Superconductors (HTS)

The real breakthrough in High-Temperature Superconductors (HTS), also known as High T_c superconductors, commenced in 1987 at the IBM research laboratory in Zurich, Switzerland, courtesy of Bednorz and Müller. A novel type of lanthanum copper oxides (LaBaCuO) compound was revealed, exhibiting superconductivity up to 35 K. This surpassed the theoretical forecast made two decades earlier, which had predicted 30 K. (Bednorz et al., 1986). Subsequently, this initial discovery of cuprates received the Nobel Prize in Physics a year later. This groundbreaking revelation

© COPYRIGHT UPM

sparked immense interest among researchers worldwide, encouraging intensified exploration of various chemical compounds in the realm of HTS due to their significantly enhanced superconducting properties (Cava et al., 1987).

During the initial months of 1987, research teams from the University of Alabama and Houston, led by M. K. Wu and P. W. Chu, discovered superconductivity in $YBa_2Cu_3O_{7-\delta}$ (YBCO) at 92 K, which notably exceeded the boiling point of liquid nitrogen at 77 K (Ching Wu Chu, 1988). Following the revelation of superconductivity in cuprates, laboratories worldwide initiated an intense pursuit aimed at raising the transition temperature beyond the boiling point of liquid nitrogen (77 K), achieved through the discovery of YBCO. This marked the first instance of a superconductor with $T_c > 77K$, reaching up to 130K in mercury-based compounds under pressure. The advent of YBCO's discovery sparked a significant surge in research endeavors. Its role in the HTS system became pivotal. It was recognised as the first to exhibit superconductivity above the boiling point of liquid nitrogen, a notably more cost-effective and manageable alternative to the expensive and challenging liquid helium. The system's granular nature and the material's intriguing behaviour, even at room temperature, became a focal point for researchers.

1.3 Research Innovation

This research delves into the thermodynamic fluctuations of the YBCO system, which play a crucial role in its fundamental properties. It involves analyzing excess conductivity, providing detailed insights into the transition to the superconducting state from temperatures well above T_c. This enables the exploration of fluctuations in

© COPYRIGHT UPM

superconducting Cooper pairs across a wide temperature range beyond T_c, allowing for experimental access to several microscopic properties of high-temperature superconducting materials. Moreover, the research emphasizes a sustainable method by incorporating environmentally friendly organic polymers, such as chitosan obtained from marine waste, and calcium compounds extracted from chicken eggshells, into the YBCO system through a green synthesis thermal treatment approach. This process is conducted entirely in an oxygen atmosphere and under ambient conditions, resulting in improved superconducting properties. This research marks a notable technological progression by integrating renewable energy sources into the fabrication of high-temperature superconductors. This not only caters to the demands of environmentally conscious high-field technological applications but also aids in tackling the global issue of waste management.

1.4 Problem Statement

The challenge lies in enhancing the quality of Y-123 systems by addressing issues such as reduced conductivity at grain boundaries and weak flux pinning within the compound. Weak link behavior in Y-123 is attributed to structural inhomogeneities and the presence of non-superconducting phases at grain boundaries, impacting inter-grain connectivity. Weak inter-grain links and limited flux pinning capability contribute to lower critical current density (J_c) values in bulk specimens, primarily due to these weak links. Additionally, Y-123 exhibits reduced anisotropy and relatively lower transition temperature (T_c), which affects the width of the transition temperature (ΔT_c and $\Delta T_c^{\text{MF-offset}}$), and its ability to sustain a significant J_c. Efforts to improve ΔT_c and $\Delta T_c^{\text{MF-offset}}$, or J_c have focused on introducing artificial pinning centers (APCs)

© COPYRIGHT UPM

such as alkali earth metal (Calcium) into the copper oxide system (Feighan et al., 2017; Murakami et al., 1989). Overcoming these challenges and achieving significant superconducting properties depends on controlling the macrostructure and microstructure of bulk samples, which affect the electrical properties within and between grains of the superconducting material. The optimal microstructure size for an effective trapping center depends on its preparation, growth mechanism, and intentional creation of well-connected defects during the growth process. Despite numerous efforts, understanding the mechanism behind Y-123 and its superconducting properties remains elusive. Research focusing on investigating thermodynamic fluctuations, specifically the excess conductivity above T_c, continues to be a key area in high-temperature superconductors (HTS) research. This aims to uncover the precise mechanism governing superconductivity through intra-grain and inter-grain properties of these materials. Excess conductivity, identified as the deviation from the linear relationship between resistance and temperature above T_c in HTS, has been linked to fluctuations in the superconducting order parameter (Ghorbani et al., 2014). Studying excess conductivity resulting from thermodynamic fluctuations provides valuable insights into fundamental aspects, including a deeper understanding of intrinsic superconducting characteristics (internal defects in the structure), the dimensionality of HTS systems, as well as extrinsic properties of the specimens such as grain morphology and grain coupling (Slimani et al., 2024).

1.5 Objectives of Research

The main goal of this project is to investigate the unique effects of thermal fluctuation and excess conductivity properties resulting from the addition of different

© COPYRIGHT UPM

concentrations of chitosan derived from marine waste, commercially sourced CaO, and Ca-based compounds extracted from chicken eggshells (ranging from concentrations, x = 0.0000 wt.% to 0.6000 wt.%) into $YBa_2Cu_3O_{7-y}$ specimens using a green approach thermal treatment method.

This main objective can be divided as follows:

i. To optimize the phase formation of $(YBCO)_{1-x}(chitosan)_x$, $(YBCO)_{1-x}(CaO)_x$, and $(YBCO)_{1-x}(Ca\ compounds)_x$ prepared using thermal treatment method.

ii. To investigate the superconducting properties resulting from thermodynamic fluctuations, especially focusing on the excess conductivity properties of $(YBCO)_{1-x}(chitosan)_x$, $(YBCO)_{1-x}(CaO)_x$, and $(YBCO)_{1-x}(Ca\ compounds)_x$.

iii. To establish the structural relationship between microstructure morphology and the conductivity induced by thermodynamic fluctuations in the specimens.

1.6 Motivation for Incorporating Chitosan (Waste Marine Extraction), CaO, and Ca Compounds (Chicken Eggshells Extraction) into YBCO System

The rapid growth of industries and population has led to the creation and lasting presence of diverse inorganic and organic pollutants, posing potential hazards to both the environment and human well-being. Mitigating these pollutants from environmental sources like air, water, and soil has become a critical global challenge, prompting the development of various nanotechnologies and nanostructured materials for effective environmental cleanup. The contrast between global waste disposal challenges and the advancement of high-field technology leads to varied perspectives in research as follows:

© COPYRIGHT UPM

- Environmental Impact: Some argue that while high-field technology advancements are beneficial, they also generate electronic waste and byproducts, contributing to the pressing issue of waste disposal and posing environmental risks if not managed properly.
- Technological Innovation: Advocates of high-field technology development highlight its crucial role in scientific, medical, and industrial advancements. Prioritizing technological progress can spur innovation and contribute to solving environmental issues through more efficient waste management technologies, as suggested.
- Sustainability Concerns: Critics emphasize that the rapid evolution of high-field technology might outpace sustainable waste disposal solutions. There is a stress on the need for concurrent research and investment in sustainable materials, recycling, and waste management strategies to counterbalance the environmental impact of technological advancement.

The motivation behind incorporating chitosan extracted from marine waste and calcium compounds from eggshells into the YBCO system for this study stems from their environmental advantages and unique properties. These materials are biodegradable, have a minimal environmental impact, and offer potential for waste reduction. They also exhibit properties that can enhance YBCO superconductors, such as acting as effective pinning centers or improving the material's microstructure. Previous research has shown their effectiveness in similar applications (Aranaz et al., 2021; Awana et al., 1994; Guth et al., 2001; Hammerl et al., 2000; Jampafuang et al., 2019; Khoerunnisa et al., 2023; Khoerunnisa et al., 2021; Kucera et al., 1995; Mohan et al., 2007; Swethavinayagam et al., 2019), highlighting the importance of sustainable

© COPYRIGHT UPM

materials and environmentally friendly practices in high-field technology development. Commercially sourced CaO is also added to the YBCO system as a benchmark for comparing the effectiveness of the calcium compounds derived from chicken eggshells.

These different opinions show how tricky it is to balance progress with dealing with global waste. The goal of research here is to improve technology while keeping waste under control and being kind to the environment. Superconducting Magnetic Energy Storage (SMES) systems are an example of this. They're eco-friendly, not needing to burn carbon or disrupt the environment with things like building dams. But the strong magnetic fields they produce need safety measures. SMES systems are great for tasks needing lots of energy quickly, like defense lasers. They're really efficient, losing only a bit of energy when converting from DC to AC and during cooling (Abd-Shukor, 2004).

1.7 Research Impact on Society, Economy and Nation

This substance has the potential to boost energy efficiency, establish cost-effective safety measures for various energy storage systems in Malaysia, and cut down maintenance costs for hospital Magnetic Resonance Imaging (MRI) systems nationwide. The research also elevates intellectual and industrial contributions by investigating the superconducting properties using an eco-friendly approach to produce bulk Rear-earth Barium Copper Oxide (REBCO). The development and fabrication process of bulk REBCO via an innovative thermal treatment method have

© COPYRIGHT UPM

demonstrated enhanced superconducting properties for large-scale industrial applications in manufacturing bulk REBCO.

1.8 Potential Applications for High-Temperature Superconductors

Understanding the superconducting properties of cuprate oxide superconductors continues to pose a complex challenge. Yet, substantial progress has been made in leveraging their practical uses, largely owing to advancements in materials science and processing. These materials have gained recognition for their significance in high-field applications, finding use in superconducting bearings, flywheel energy storage systems, and large-scale bulk superconducting magnets.

In the past twenty years, significant advancements have emerged in the physics of superconductivity, primarily driven by the discovery and extensive exploration of HTS. These novel materials have unveiled promising potential for diverse applications in advanced technologies and high-field applications. Generally, the applications of HTS can be categorized into two groups: large-scale and small-scale (refer Figure 1.5). Moreover, Small scale applications are expected to be commercialized earlier than large scale applications.

High-temperature superconductors (HTS) intended for large-scale applications must possess both a high J_c and the ability to endure the stresses generated by high magnetic fields. Large-scale applications encompass several key high-field applications (Abd-Shukor, 2004), as outlined below:

© COPYRIGHT UPM

✓ Medical applications: Magnetic Resonance Imaging (MRI), biotechnical engineering, super magnets (powerful superconducting magnet) for diagnostics medicine such as nuclear spin tomographs, superconducting accelerators applications, high field magnets

✓ Power generation: motors, generators, flywheel energy storage system, transmission, fusion, transformers and inductors, power transmission cables, fusion confinement

✓ Transport system and industry: magnetically levitated vehicles (MAGLEV), marine propulsion system, magnetic separator, kinetic launch vehicles

Typically, small-scale applications necessitate thin films and commonly employed deposition techniques such as:

✓ Electronics: Superconducting Quantum Interferences Devices (SQUIDs), transistors, Josephson junction devices, wires and circuitry connections, particle accelerators, sensors, resonators, microwave devices (filters / resonators), radiation detectors, magnetics field detectors, computers

✓ Industrial: separation, magnets, sensors and transducers, magnetic shielding, superconducting bearings

© COPYRIGHT UPM

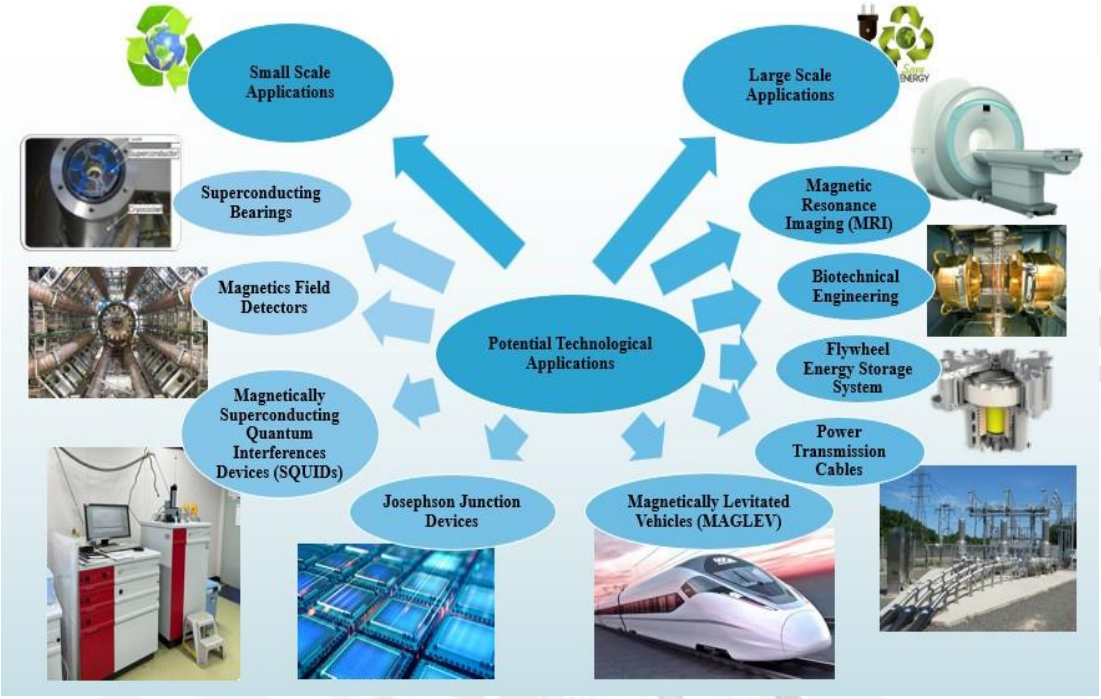

Figure 1.5: The potential technological applications of High-Temperature Superconductors ("Superconducting chips to scale up quantum computers and boost supercomputers," 2021; Chu, 2023; Français, 2006; Marquis, 2016)

1.9 Thesis Outlook and Overview

This thesis comprises six chapters. Chapter 1 provides a succinct overview of superconductors and their potential applications, addressing the problem statement, objectives of this work, as well as the innovation and commercial value of this research. The chapter concludes by discussing the global issue versus the development of high-field technology. In Chapter 2, a review of previous studies on the Cuprates Family, particularly YBCO, focuses on the thermal treatment methods and dopant additions employed by earlier researchers. Additionally, a comprehensive review of the positive outcomes resulting from thermal fluctuation-induced excess conductivity analysis in previous research is also undertaken. Chapter 3 will intricately detail the theory and fundamentals of superconductivity, especially concerning YBCO. Chapter

© COPYRIGHT

4 centers on the materials and methods utilized in this study, providing detailed discussions on sample characterization methods such as XRD, FESEM, and DC resistivity measurement. Chapter 5 comprehensively analyses the results obtained from sample characterizations. Finally, Chapter 6 consolidates the research outcomes and presents recommendations for future research pursuits.

© COPYRIGHT UPM

REFERENCES

Abd-Shukor, R. (2004). *Introduction to Superconductivity in Metals, Alloys & Cuprates* (P. U. P. S. I. T. Malim Ed.).

Abou-Aly, A. I., Awad, R., Ibrahim, I. H., & Abdeen, W. (2009). Excess conductivity analysis for $Tl_{0.8}Hg_{0.2}Ba_2Ca_2Cu_3O_{9-\delta}$ substituted by Sm and Yb. *Solid State Communications, 149*(7), 281-285.

Abou Aly, A. I., Mohammed, N. H., Awad, R., Motaweh, H. A., & El-Said Bakeer, D. (2012). Determination of Superconducting Parameters of $GdBa_2Cu_3O_{7-\delta}$ Added with Nanosized Ferrite CoFe2O4 from Excess Conductivity Analysis. *Journal of Superconductivity and Novel Magnetism, 25*(7), 2281-2290.

Abrikosov, A. A. (2001). Properties of the pseudogap phase in high T_c superconductors. *Physical Review B, 64*(10), 104521.

Agassi, D., Christen, D., & Pennycook, S. (2002). Flux pinning and critical currents at low-angle grain boundaries in high-temperature superconductors. *Applied Physics Letters, 81*(15), 2803-2805.

Aksan, M. A., Kizilaslan, O., Aksan, E. N., & Yakinci, M. E. (2012). Thermoelectric power and thermal conductivity study of the $Y_3Ba_5Cu_8O_x$ system. *Physica B: Condensed Matter, 407*(14), 2820-2824.

Akyol, M., Ayaş, A. O., Akça, G., Çetin, S. K., & Ekicibil, A. (2015). Effect of Ca doping on thermally activated flux flow in the $Y_3Ba_5Cu_8O_{18}$ superconductor. *Bulletin of Materials Science, 38*(5), 1231-1237.

Al-Hada, N. M., Saion, E., Kamari, H. M., Flaifel, M. H., Shaari, A. H., Talib, Z. A., Abdullahi, N., Baqer, A. A., & Kharazmi, A. (2016). Structural, morphological and optical behaviour of PVP capped binary $(ZnO)_{0.4}$ $(CdO)_{0.6}$ nanoparticles synthesised by a facile thermal route. *Materials Science in Semiconductor Processing, 53*, 56-65.

Al-Hada, N. M., Saion, E., Talib, Z. A., & Shaari, A. H. (2016). The impact of polyvinylpyrrolidone on properties of cadmium oxide semiconductor nanoparticles manufactured by heat treatment technique. *Polymers, 8*(4), 113.

Al-Hada, N. M., Saion, E. B., Shaari, A. H., Kamarudin, M. A., Flaifel, M. H., Ahmad, S. H., & Gene, S. A. (2014). A facile thermal-treatment route to synthesize ZnO nanosheets and effect of calcination temperature. *PloS One, 9*(8), e103134.

Al-Sharabi, A., & Abd-Shukor, R. (2014). Excess conductivity analysis of Cr substituted $TlSr_2CaCu_2O_{7-\delta}$ superconductor at Tl and Ca sites. *Journal of Alloys and Compounds, 615*, 363-371.

Al-Sharabi, A., Tajuddin, S. Y., Saffiey, A. D. F. W., & Jasman, S. (2016). Analisis kekonduksian lebihan superkonduktor $YBa_2Cu_3O_{7-\delta}$ ditambah nanozarah PbO. *Sains Malaysiana, 45*(12), 1959-1969.

Alloul, H., Rullier-Albenque, F., Vignolle, B., Colson, D., & Forget, A. (2010). Superconducting fluctuations, pseudogap and phase diagram in cuprates. *Europhysics Letters, 91*(3), 37005.

Almessiere, M. A., Hannachi, E., Slimani, Y., Yasin, G., Mumtaz, M., Koblischka, M. R., Koblischka-Veneva, A., Manikandan, A., & Baykal, A. (2020). Dimensionality and superconducting parameters of $YBa_2Cu_3O_{7-d}/(WO_3\ NPs)_x$ composites deduced from excess conductivity analysis. *Materials Chemistry and Physics, 243*, 122665.

Aranaz, I., Alcántara, A. R., Civera, M. C., Arias, C., Elorza, B., Heras Caballero, A., & Acosta, N. (2021). Chitosan: an overview of its properties and applications. *Polymers, 13*(19), 3256.

Aslamasov, L., & Larkin, A. (1968). The influence of fluctuation pairing of electrons on the conductivity of normal metal. *Physics Letters A, 26*(6), 238-239.

Aslamazov, L. (1969). Influence of impurities on the existence of an inhomogeneous state in a ferromagnetic superconductor. *Soviet Physics-JETP (Translation of Zhurnal Eksperimental`noi i Teoretischeskoi Fiziki), 28*(4), 773-775.

Aslamazov, L., & Larkin, A. (1968). Effect of fluctuations on the properties of a superconductor above the critical temperature. *Sovient Physics - Solid State, 10*(4), 23-28.

Awana, V., & Narlikar, A. (1994). Role of calcium in suppressing the superconductivity of $Y_{1-x}Ca_xBa_2Cu_3O_{7-\delta}$. *Physical Review B, 49*(9), 6353.

Babic, E., Prester, M., Marohnić, Ž., Car, T., Biškup, N., & Siddiqi, S. A. (1989). Critical currents and differential resistance of $YBa_2Cu_3O_{7-x}$ superconducting ceramics. *Solid State Communications, 72*(8), 753-757.

Bahboh, A., Shaari, A. H., Baqiah, H., Kien, C. S., Kechik, M. M. A., Wahid, M. H., Abd-Shukor, R., & Talib, Z. A. (2019). Effects of $HoMnO_3$ nanoparticles addition on microstructural, superconducting and dielectric properties of $YBa_2Cu_3O_{7-\delta}$. *Ceramics International, 45*(11), 13732-13739.

Barood, F., Awang Kechik, M. M., Miryala, M., Soo Kien, C., Kean Pah, L., Halim Shaari, A., & Baqiah, H. (2024). Effect of annealing temperature condition on the phase formation and electric proeprties of $YBa_2Cu_3O_{7-\delta}$ superconductor synthesised by thermal treatment method. *Solid State Science and Technology, 31*(2), 63-70.

Barood, F., Kechik, M. M. A., Tee, T. S., Kien, C. S., Pah, L. K., Hong, K. J., Shaari, A. H., Baqiah, H., Karim, M. K. A., Shabdin, M. K., Mohd Shariff, K. K., Hashim, A., Suhaimi, N. E., & Miryala, M. (2023). Orthorhombic $YBa_2Cu_3O_{7-\delta}$ superconductor with TiO_2 nanoparticle addition: crystal structure, electric resistivity, and AC susceptibility. *Coatings, 13*(6), 1093.

© COPYRIGHT UPM

Bednorz, J. G., & Müller, K. A. (1986). Possible high Tc superconductivity in the Ba−La−Cu−O system. *Zeitschrift fur Physik B Condensed Matter, 64*(2), 189-193.

Behera, D., & Mishra, N. C. (2002). Granularity controlled percolative current conduction in $YBa_2Cu_3O_7$ / Ag composite thick films. *Superconductor Science and Technology, 15*(1), 72.

Benzi, P., Bottizzo, E., & Rizzi, N. (2004). Oxygen determination from cell dimensions in YBCO superconductors. *Journal of Crystal Growth, 269*(2), 625-629.

Berenov, A., Farvacque, C., Qi, X., MacManus-Driscoll, J., MacPhail, D., & Foltyn, S. (2002). Ca doping of YBCO grain boundaries. *Physica C: Superconductivity, 372*, 1059-1062.

Bhargava, A., Mackinnon, I. D. R., Yamashita, T., & Page, D. (1995). Bulk manufacture of YBCO powders by coprecipitation. *Physica C: Superconductivity, 241*(1), 53-62.

Bianconi, A., Valletta, A., Perali, A., & Saini, N. L. (1998). Superconductivity of a striped phase at the atomic limit. *Physica C: Superconductivity, 296*(3), 269-280.

Billah, A. (2016). *Investigation of multiferroic and photocatalytic properties of Li doped $BiFeO_3$ nanoparticles prepared by ultrasonication.*

Boston, R., Awaya, K., Nakayama, T., Ogasawara, W., & Hall, S. R. (2014). Formation of superconducting yttrium barium copper oxide using sulphur-containing templates. *RSC Advances, 4*(51), 26824-26828.

Böttger, G., Mangelschots, I., Kaldis, E., Fischer, P., Ch, K., & Fauth, F. (1996). The influence of Ca doping on the crystal structure and superconductivity of orthorhombic. *Journal of Physics: Condensed Matter, 8*(45), 8889.

Böttger, G., Schwer, H., Kaldis, E., & Bente, K. (1997). Ca doping of $YBa_2Cu_3O_{7-\sigma}$ single crystals: structural aspects. *Physica C: Superconductivity, 275*(3-4), 198-204.

Bottom, R. (2008). Thermogravimetric analysis. *Principles and Applications of Thermal Analysis*, 87-118.

Bouchoucha, I., Ben Azzouz, F., & Ben Salem, M. (2011). Excess conductivity studies in $Zn_{0.95}Mn_{0.05}O$ and ZnO added $YBa_2Cu_3O_y$ superconductors. *Journal of Superconductivity and Novel Magnetism, 24*(1), 345-350.

Bulk Nanostructured Metals. (2010). Retrieved from http://www.bnm.mtl.kyoto-u.ac.jp/outline/background_e.html

Bungre, S. S., Meisels, R., Shen, Z. X., & Caplin, A. D. (1989). Are classical weak-link models adequate to explain the current–voltage characteristics in bulk $YBa_2Cu_3O_{7-\delta}$. *Nature, 341*(6244), 725-727.

© COPYRIGHT UPM

Calore, L., Rahman Khan, M. M., Cagliero, S., Agostino, A., Truccato, M., & Operti, L. (2013). Al doping influence on crystal growth, structure and superconducting properties of Y(Ca)$Ba_2Cu_3O_{7-y}$ whiskers. *Journal of Alloys and Compounds, 551*, 19-23.

Capponi, J., Chaillout, C., Hewat, A., Lejay, P., Marezio, M., Nguyen, N., Raveau, B., Soubeyroux, J., Tholence, J., & Tournier, R. (1987). Structure of the 100 K superconductor $Ba_2YCu_3O_7$ between (5 - 300) K by neutron powder diffraction. *EPL (Europhysics Letters), 3*(12), 1301.

Cava, R., Hewat, A., Hewat, E., Batlogg, B., Marezio, M., Rabe, K., Krajewski, J., Peck Jr, W., & Rupp Jr, L. (1990). Structural anomalies, oxygen ordering and superconductivity in oxygen deficient $Ba_2YCu_3O_x$. *Physica C: Superconductivity, 165*(5-6), 419-433.

Cava, R. J., Batlogg, B., Van Dover, R., Murphy, D., Sunshine, S., Siegrist, T., Remeika, J., Rietman, E., Zahurak, S., & Espinosa, G. (1987). Bulk superconductivity at 91 K in single-phase oxygen-deficient perovskite $Ba_2YCu_3O_{9-\delta}$. *Physical Review Letters, 58*(16), 1676.

Ching Wu Chu, P. (1988). The discovery and physics of superconductivity above 100 K. *AIP Conference Proceedings, 169*(1), 220-240.

Chu, J. (2023). Physicists discover a new switch for superconductivity. Retrieved from https://phys.org/news/2023-06-physicists-superconductivity.html

Civale, L. (1997). Vortex pinning and creep in high-temperature superconductors with columnar defects. *Superconductor Science and Technology, 10*(7A), A11.

Claus, H., Gebhard, U., Linker, G., Röhberg, K., Riedling, S., Franz, J., Ishida, T., Erb, A., Müller-Vogt, G., & Wühl, H. (1992). Phase separation in $YBa_2Cu_3O_{7-\delta}$ single crystals near $\delta = 0$. *Physica C: Superconductivity, 200*(3-4), 271-276.

Dadras, S., Davoudiniya, M., & Dehghani, S. (2017). Investigation and comparing the effects of CNTs and Ag nanoparticles doping on YBCO superconductor properties. *Journal of Superconductivity and Novel Magnetism, 30*(9), 2451-2456.

Daeumling, M., Seuntjens, J., & Larbalestier, D. (1990). Oxygen-defect flux pinning, anomalous magnetization and intra-grain granularity in $YBa_2Cu_30_{7-\delta}$. *Nature, 346*(6282), 332-335.

Danks, A. E., Hall, S. R., & Schnepp, Z. (2016). The evolution of 'sol–gel' chemistry as a technique for materials synthesis. *Materials Horizons, 3*(2), 91-112.

Demirel, A. I. (2004). Pinning mechanism and flux motion in $YBa_2Cu_3O_7$ thin films. *International Journal of Modern Physics B, 18*(07), 999-1006.

Diab, M. A., El-Sonbati, A. Z., & Bader, D. M. D. (2011). Thermal stability and degradation of chitosan modified by benzophenone. *Spectrochimica Acta, Part A: Molecular and Biomolecular Spectroscopy, 79*(5), 1057-1062.

© COPYRIGHT UPM

Díaz, A., Maza, J., & Vidal, F. (1997). Anisotropy and structural-defect contributions to percolative conduction in granular copper oxide superconductors. *Physical Review B, 55*(2), 1209.

Dihom, M. M., Shaari, A. H., Baqiah, H., Al-Hada, N. M., Chen, S. K., Azis, R. a. S., Awang Kechik, M. M., & Abd-Shukor, R. (2017). Effects of calcination temperature on microstructure and superconducting properties of Y123 ceramic prepared using thermal treatment method. *Solid State Phenomena, 268*, 325-329.

Dihom, M. M., Shaari, A. H., Baqiah, H., Al-Hada, N. M., Chen, S. K., Kechik, M. M. A., & Abd-Shukor, R. (2017). *Effects of calcination temperature on microstructure and superconducting properties of Y123 ceramic prepared using thermal treatment method.* Paper presented at the Solid State Phenomena.

Dihom, M. M., Shaari, A. H., Baqiah, H., Al-Hada, N. M., Kien, C. S., Azis, R. S., Kechik, M. M. A., Talib, Z. A., & Abd-Shukor, R. (2017). Microstructure and superconducting properties of Ca substituted Y(Ba1−Ca)2Cu3O7−δ ceramics prepared by thermal treatment method. *Results in Physics, 7*, 407-412.

Dihom, M. M., Shaari, A. H., Baqiah, H., Al-Hada, N. M., Kien, C. S., Azis, R. S., Kechik, M. M. A., Talib, Z. A., & Abd-Shukor, R. (2017). Microstructure and superconducting properties of Ca substituted $Y(Ba_{1-x}Ca_x)_2Cu_3O_{7-\delta}$ ceramics prepared by thermal treatment method. *Results in Physics, 7*, 407-412.

Dihom, M. M., Shaari, A. H., Baqiah, H., Al-Hada, N. M., Talib, Z. A., Kien, C. S., Azis, R. S., Kechik, M. M. A., Pah, L. K., & Abd-Shukor, R. (2017). Structural and superconducting properties of $Y(Ba_{1-x}K_x)_2Cu_3O_{7-\delta}$ ceramics. *Ceramics International, 43*(14), 11339-11344.

Dihom, M. M., Shaari, A. H., Baqiah, H., Kien, C. S., Azis, R. S., Abd-Shukor, R., Al-Hada, N. M., Kechik, M. M. A., & Talib, Z. A. (2019). Calcium-substituted $Y_3Ba_5Cu_8O_{18}$ ceramics synthesized via thermal treatment method: structural and superconducting properties. *Journal of Superconductivity and Novel Magnetism, 32*(7), 1875-1883.

Dimos, D., Chaudhari, P., & Mannhart, J. (1990). Superconducting transport properties of grain boundaries in $YBa_2Cu_3O_7$ bicrystals. *Physical Review B, 41*(7), 4038.

Dubinsky, S., Lumelsky, Y., Grader, G. S., Shter, G. E., & Silverstein, M. S. (2005). Thermal degradation of poly (acrylic acid) containing metal nitrates and the formation of $YBa_2Cu_3O_{7-X}$. *Journal of Polymer Science Part B: Polymer Physics, 43*(10), 1168-1176.

Dzul-Kifli, N. A. C., Kechik, M. M. A., Baqiah, H., Shaari, A. H., Lim, K. P., Chen, S. K., Sukor, S. I. A., Shabdin, M. K., Karim, M. K. A., Shariff, K. K. M., & Miryala, M. (2022). Superconducting properties of $YBa_2Cu_3O_{7-\delta}$ with a multiferroic addition synthesized by a capping agent-aided thermal treatment method. *Nanomaterials, 12*(22), 3958.

© COPYRIGHT UPM

Elton, L. R. B., & Jackson, D. F. (1966). X-Ray diffraction and the Bragg Law. *American Journal of Physics, 34*(11), 1036-1038.

Feighan, J., Kursumovic, A., & MacManus-Driscoll, J. (2017). Materials design for artificial pinning centres in superconductor PLD coated conductors. *Superconductor Science and Technology, 30*(12), 123001.

Français, V. e. (2006). World's largest superconducting magnet switches on. Retrieved from https://home.web.cern.ch/news/press-release/cern/worlds-largest-superconducting-magnet-switches

Freitas, P. P., Tsuei, C. C., & Plaskett, T. S. (1987). Thermodynamic fluctuations in the superconductor $Y_1Ba_2Cu_3O_{9-y}$ Evidence for three-dimensional superconductivity. *Physical Review B, 36*(1), 833-835.

Ghorbani, S. R., & Rahmati Tarki, M. (2014). Fluctuation conductivity of $RE_{1-2x}Ca_xM_xBa_2Cu_3O_{7-\delta}$(RE=Nd, Y and M=Pr, Th) superconductors. *Journal of Superconductivity and Novel Magnetism, 27*(3), 749-754.

Ghosh, A. K., Bandyopadhyay, S. K., Barat, P., Sen, P., & Basu, A. N. (1995). Excess-conductivity analysis of α irradiated polycrystalline Bi-2212 superconductor. *Physica C: Superconductivity, 255*(3), 319-323.

Ginzburg, V., & Landau, L. (1950). Zh. eksper. teor. *Fizika, 20*(1064), 1960.

Giri, R., Awana, V., Singh, H., Tiwari, R., Srivastava, O., Gupta, A., Kumaraswamy, B., & Kishan, H. (2005). Effect of Ca doping for Y on structural/microstructural and superconducting properties of $YBa_2Cu_3O_{7-\delta}$. *Physica C: Superconductivity and its Applications, 419*(3-4), 101-108.

Goodman, B. B. (1966). Type II superconductors. *Reports on Progress in Physics, 29*(2), 445.

Guth, K., Krebs, H., Freyhardt, H., & Jooss, C. (2001). Modification of transport properties in low-angle grain boundaries via calcium doping of $YBa_2Cu_3O_\delta$ thin films. *Physical Review B, 64*(14), 140508.

Gyurov, G., Khristova, I., Peshev, P., & Abrashev, M. (1993). Preparation of a calcium-substituted copper-rich yttrium barium copper oxide superconductor from a spray-dried nitrate precursor. *Materials Research Bulletin, 28*(10), 1067-1074.

Hall, S. R. (2006). Biomimetic synthesis of high-T_c, type-II superconductor Nanowires. *Advanced Materials, 18*(4), 487-490.

Hamadneh, I., Rosli, A. M., Abd-Shukor, R., Suib, N. R. M., & Yahya, S. Y. (2008). Superconductivity of $REBa_2Cu_3O_{7-\delta}$ (RE= Y, Dy, Er) ceramic synthesized via coprecipitation method. *Journal of Physics: Conference Series, 97*, 012063.

Hammerl, G., Schmehl, A., Schulz, R. R., Götz, B., Bielefeldt, H., Schneider, C. W., Hilgenkamp, H., & Mannhart, J. (2000). Enhanced supercurrent density in

© COPYRIGHT UPM

polycrystalline $YBa_2Cu_3O_{7-\delta}$ at 77 K from calcium doping of grain boundaries. *Nature, 407*(6801), 162-164.

Hannachi, E., Slimani, Y., Almessiere, M. A., Alotaibi, S. A., Omelchenko, L. V., Petrenko, E. V., Kurbanov, U., Ben Azzouz, F., Solovjov, A. L., & Baykal, A. (2023). YBCO polycrystal co-added with $BaTiO_3$ and WO_3 nanoparticles: Fluctuation induced conductivity and pseudogap studies. *Current Applied Physics, 48*, 70-78.

Hannachi, E., Slimani, Y., Azzouz, F. B., & Ekicibil, A. (2018). Higher intra-granular and inter-granular performances of YBCO superconductor with TiO_2 nano-sized particles addition. *Ceramics International, 44*(15), 18836-18843.

Hannachi, E., Slimani, Y., Ben Salem, M. K., Hamrita, A., Al-Otaibi, A. L., Almessiere, M. A., Ben Salem, M., & Ben Azzouz, F. (2016). Fluctuation induced conductivity studies in $YBa_2Cu_3O_y$ compound embedded by superconducting nano-particles Y-deficient $YBa_2Cu_3O_y$: effect of silver inclusion. *Indian Journal of Physics, 90*(9), 1009-1018.

Hannachi, E., Slimani, Y., Ekicibil, A., Manikandan, A., & Azzouz, F. B. (2019). Excess conductivity and AC susceptibility studies of Y-123 superconductor added with TiO_2 nano-wires. *Materials Chemistry and Physics, 235*, 121721.

Hannachi, E., Slimani, Y., Ekicibil, A., Manikandan, A., & Azzouz, F. B. (2019). Magneto-resistivity and magnetization investigations of YBCO superconductor added by nano-wires and nano-particles of titanium oxide. *Journal of Materials Science: Materials in Electronics, 30*(9), 8805-8813.

Hapipi, N. M., Chen, S. K., Shaari, A. H., Kechik, M. M. A., Tan, K. B., & Lim, K. P. (2018). Superconductivity of Y_2O_3 and $BaZrO_3$ nanoparticles co-added $YBa_2Cu_3O_{7-\delta}$ bulks prepared using co-precipitation method. *Journal of Materials Science: Materials in Electronics, 29*(21), 18684-18692.

Hapipi, N. M., Chen, S. K., Shaari, A. H., Kechik, M. M. A., Tan, K. B., Lim, K. P., & Lee, O. J. (2019). AC susceptibility of $BaZrO_3$ nanoparticles added $YBa_2Cu_3O_{7-\delta}$ superconductor prepared via coprecipitation method. *Journal of Superconductivity and Novel Magnetism, 32*(5), 1191-1198.

Harabor, A., Harabor, N., & Deletter, M. (2006). Short-wavelength fluctuation regime in paraconductivity of bulk monophase (Bi, Pb)-2223 superconductor system. *Journal of Optoelectronics and Advanced Materials, 8*(3), 1072.

Hashim, A., Norazidah, A. W., Kasim, A., Nazree, A., Syamsyir, S. A., Hidayah, H. N., & Hawa, J. S. (2016). Electrical and structural properties of Ca substitution in high and low density Y $(Ba_{1-x}Ca_x)_2Cu_3O_{7-\delta}$ superconductor. *Materials Science Forum, 846*, 586-590.

Hatada, K., & Shimizu, H. (1998). Structural and superconducting properties of $R_{1-x}CaxBa_2Cu_3O_{6+\delta}$ (R=Y, Er, Gd, Eu; $0<\delta<1$). *Physica C: Superconductivity, 304*(1), 89-95.

© COPYRIGHT UPM

Haugan, T., Campbell, T., Pierce, N., Locke, M., Maartense, I., & Barnes, P. (2008). Microstructural and superconducting properties of $(Y_{1-x}Eu_x)Ba_2Cu_3O_{7-\delta}$ thin films: x= 0–1. *Superconductor Science and Technology, 21*(2), 025014.

Hidayah, H., Yahya, S., Azhan, H., Azman, K., Hawa, J., & Norazidah, A. (2012). *Effect of Ca substitution at Y-site of $YB_2C_3O_7$ sSuperconductor prepared via co-precipitation method.* Paper presented at the Advanced Materials Research.

Holesinger, T. G., Civale, L., Maiorov, B., Feldmann, D. M., Coulter, J. Y., Miller, D. J., Maroni, V. A., Chen, Z., Larbalestier, D. C., Feenstra, R., Li, X., Huang, Y., Kodenkandath, T., Zhang, W., Rupich, M. W., & Malozemoff, A. P. (2008). Progress in nanoengineered microstructures for tunable high-current, high-temperature superconducting wires. *Advanced Materials, 20*(3), 391-407.

Huang, S.-L., Koblischka, M. R., Fossheim, K., Ebbesen, T. W., & Johansen, T. H. (1999). Microstructure and flux distribution in both pure and carbon-nanotube-embedded $Bi_2Sr_2CaCu_2O_{8+\delta}$ superconductors. *Physica C: Superconductivity, 311*(3), 172-186.

Isfort, D., Chaud, X., Tournier, R., & Kapelski, G. (2003). Cracking and oxygenation of YBaCuO bulk superconductors: application to c-axis elements for current limitation. *Physica C: Superconductivity, 390*(4), 341-355.

Jablonsky, M., Haz, A., Orsagova, & Surina, I. (2013). *Determination of temperature regions in thermal degradation of lignin*.

Jampafuang, Y., Tongta, A., & Waiprib, Y. (2019). Impact of crystalline structural differences between α- and β-chitosan on their nanoparticle formation via ionic gelation and superoxide radical scavenging activities. *Fibers and Polymers, 11*(12), 2010.

Janod, E., Junod, A., Graf, T., Wang, K. Q., Triscone, G., & Muller, J. (1993). Split superconducting transitions in the specific heat and magnetic susceptibility of $YBa_2Cu_3O_x$ versus oxygen content. *Physica C: Superconductivity, 216*(1), 129-139.

Jasim, S. E., Jusoh, M. A., Hafiz, M., & Jose, R. (2016). Fabrication of superconducting YBCO nanoparticles by electrospinning. *Procedia Engineering, 148*, 243-248.

Jirák, Z., Hejtmánek, J., Pollert, E., Tříska, A., & Vašek, P. (1988). Structure and superconductivity in $Y_{1-x}Ca_xBa_2Cu_3O_7$. *Physica C: Superconductivity, 156*(5), 750-754.

Jorgensen, J., Beno, M., Hinks, D. G., Soderholm, L., Volin, K., Hitterman, R., Grace, J., Schuller, I. K., Segre, C., & Zhang, K. (1987). Oxygen ordering and the orthorhombic-to-tetragonal phase transition in Y $Ba_2Cu_3O_{7-x}$. *Physical Review B, 36*(7), 3608.

Jurelo, A. R., Castillo, I. A., Roa-Rojas, J., Ferreira, L. M., Ghivelder, L., Pureur, P., & Rodrigues, P. (1999). Coherence transition in granular high temperature superconductors. *Physica C: Superconductivity, 311*(1), 133-139.

© COPYRIGHT UPM

Kamari, H. M., Al-Hada, N. M., Saion, E., Shaari, A. H., Talib, Z. A., Flaifel, M. H., & Ahmed, A. A. A. (2017). Calcined solution-based PVP influence on ZnO semiconductor nanoparticle properties. *Crystals, 7*(2), 2.

Kamarudin, A. N., Awang Kechik, M. M., Abdullah, S. N., Baqiah, H., Chen, S. K., Abdul Karim, M. K., Ramli, A., Lim, K. P., Shaari, A. H., Miryala, M., Murakami, M., & Talib, Z. A. (2022). Effect of graphene nanoparticles addition on superconductivity of $YBa_2Cu_3O_{7-\delta}$ synthesized via the thermal treatment method. *Coatings, 12*(1), 91.

Kamarudin, A. N., Awang Kechik, M. M., Miryala, M., Pinmangkorn, S., Murakami, M., Chen, S. K., Baqiah, H., Ramli, A., Lim, K. P., & Shaari, A. H. (2021). Microstructural, phase Formation, and superconducting properties of bulk $YBa_2Cu_3O_y$ superconductors grown by infiltration growth process utilizing the $YBa_2Cu_3O_y + ErBa_2Cu_3O_y + Ba_3Cu_5O_8$ as a liquid source. *Coatings, 11*(4), 377.

Kechik, M. (2011). *Improvement of critical current density in $YBa_2Cu_3O_{7-\delta}$ films with nano-inclusions.* ([Doctorates Ph.D. dissertation]), University of Birmingham, United Kingdom: University of Birmingham.

Kechik, M., Baqiah, H., Shaari, A., WNW, W. J., Abd Sukor, S., Talib, Z., & Abd-Shukor, R. (2018). Structural and superconducting properties of thermal treatment-synthesised bulk $YBa_2Cu_3O_{7-\delta}$ superconductor: effect of addition of SnO_2 nanoparticles. *Materials (Basel, Switzerland), 12*(1).

Kechik, M. M. A., & Mohamed, A. R. A. (2024) $YBa_2Cu_3O_{7-d}$ Bulk superconductors: exploring the impact of two synthesis techniques on the microstructure and critical temperature. *Solid State Science and Technology, 32(2),* 28-41.

Khalid, N. A., Awang Kechik, M. M., Baharuddin, N. A., Kien, C. S., Baqiah, H., Pah, L. K., Shaari, A. H., Talib, Z. A., Hashim, A., & Murakami, M. (2020). Carbon nanofibers addition on transport and superconducting properties of bulk $YBa_2Cu_3O_{7-\delta}$ material prepared via co-precipitation. *Journal of Materials Science: Materials in Electronics, 31*(19), 16983-16990.

Khalid, N. A., Kechik, M. M. A., Baharuddin, N. A., Kien, C. S., Baqiah, H., Yusuf, N. N. M., Shaari, A. H., Hashim, A., & Talib, Z. A. (2018). Impact of carbon nanotubes addition on transport and superconducting properties of $YBa_2Cu_3O_{7-\delta}$ ceramics. *Ceramics International, 44*(8), 9568-9573.

Khalid, N. A., Kong, W., Kong, I., Kong, C., Kechik, M. M. A., & Abd-Shukor, R. (2021). Significance of cobalt ferrite nanoparticles onsuperconducting properties of Tl-1212 high temperature superconductor. *Nano Hybrids and Composites, 31*, 1-5.

Khan, N. A., Hassan, N., Irfan, M., & Firdous, T. (2010). Different regions of fluctuation conductivity in Sn-doped $Cu_{0.5}Tl_{0.5}Ba_2Ca_2Cu_{3-y}Sn_yO_{10-\delta}$ superconductors. *Physica B: Condensed Matter, 405*(6), 1541-1545.

Khoerunnisa, F., Amanda, P. C., Nurhayati, M., Hendrawan, H., Lestari, W. W., Sanjaya, E. H., Handayani, M., Oh, W.-D., & Lim, J. (2023). Promotional effect of ammonium chloride functionalization on the performance of

polyethersulfone/chitosan composite-based ultrafiltration membrane. *Chemical Engineering Research and Design, 190*, 366-378.

Khoerunnisa, F., Nurhayati, M., Dara, F., Rizki, R., Nasir, M., Aziz, H. A., Hendrawan, H., Poh, N. E., Kaewsaneha, C., & Opaprakasit, P. (2021). Physicochemical properties of TPP-Crosslinked chitosan nanoparticles as potential antibacterial agents. *Fibers and Polymers, 22*(11), 2954-2964.

Khoerunnisa, F., Nurhayati, M., Herlini, H., Adzkia, Q. A. A., Dara, F., Hendrawan, H., Oh, W.-D., & Lim, J. (2023). Design and application of chitosan-CuO nanocomposites synthesized via novel hybrid ionic gelation-ultrasonication methods for water disinfection. *Journal of Water Process Engineering, 52*, 103556.

Khoerunnisa, F., Sihombing, M., Nurhayati, M., Dara, F., Triadi, H. A., Nasir, M., Hendrawan, H., Pratiwi, A., Ng, E.-P., & Opaprakasit, P. (2022). Poly(ether sulfone)-based ultrafiltration membranes using chitosan/ammonium chloride to enhance permeability and antifouling properties. *Polymer Journal, 54*(4), 525-537.

Khoerunnisa, F., Yolanda, Y. D., Nurhayati, M., Zahra, F., Nasir, M., Opaprakasit, P., Choo, M.-Y., & Ng, E.-P. (2021). Ultrasonic synthesis of nanochitosan and its size effects on turbidity removal and dealkalization in wastewater treatment. *Inventions, 6*(4), 98.

Khoshnevisan, B., & Mohammadi, M. (2016). Effects of K and Ca doping on twin boundary energy of cupperate superconductors. *Physica C: Superconductivity and Its Applications, 523*, 5-9.

Khurram, A. A., Mumtaz, M., Khan, N. A., Ahadian, M. M., & Iraji-zad, A. (2007). The effect of grain size on the fluctuation-induced conductivity of $Cu_{1-x}Tl_xBa_2Ca_3Cu_4O_{12-\delta}$ superconductor thin films. *Superconductor Science and Technology, 20*(8), 742.

Koblischka, M. R., Slimani, Y., Koblischka-Veneva, A., Karwoth, T., Zeng, X., Hannachi, E., & Murakami, M. (2020). Excess conductivity analysis of polycrystalline FeSe samples with the addition of Ag. *Materials, 13*(21), 5018.

Krishnan, H., Srinivasan, R., Sankaranarayanan, V., Subramaniam, C. K., & Subba Rao, G. V. (1991). Fluctuation-induced excess conductivity in the compounds $CaREBaCu_3O_{7-y}$ (RE=La and Sm). *Bulletin of Materials Science, 14*(3), 747-752.

Kucera, J., & Bravman, J. (1995). Transport characterization of calcium-doped $YBa_2Cu_3O_{7-\delta}$ thin films. *Physical Review B, 51*(13), 8582.

Kumar, S., & Koh, J. (2012). Physiochemical, optical and biological activity of chitosan-chromone derivative for biomedical applications. *International Journal of Molecular Sciences, 13*(5), 6102-6116.

Lawrence, W., & Doniach, S. (1971). *Theory of layer-structure superconductors.* Paper presented at the Proceedings of the Twelfth International Conference on Low Temperature Physics, Tokyo Keigaku Publishing Co., Ltd.

© COPYRIGHT UPM

Lee, P. J., Saion, E., Al-Hada, N. M., & Soltani, N. (2015). A simple up-scalable thermal treatment method for synthesis of ZnO nanoparticles. *Metals, 5*(4), 2383-2392.

Leventouri, T., Soifer, G., Calamiotou, M., Perdikatsis, V., & Liarokapis, E. (1995). Ca doped YBCO on the Ba site. *Journal of Superconductivity, 8*(5), 625-626.

Loh, Z. W., Cheong, W. M., Zaid, M. H. M., Kechik, M. M. A., Fen, Y. W., Mayzan, M. Z. H., Yaakob, Y., & Liza, S. (2022). Development of fluoride-containing glass–ceramics using eggshells waste as calcium source. *Applied Physics A, 128*(10), 893.

Loh, Z. W., Mohd Zaid, M. H., Matori, K. A., Kechik, M. M. A., Fen, Y. W., Mayzan, M. Z. H., Liza, S., & Cheong, W. M. (2023). Phase transformation and mechanical properties of new bioactive glass-ceramics derived from $CaO–P_2O_5–Na_2O–B_2O_3–SiO_2$ glass system. *Journal of the Mechanical Behavior of Biomedical Materials, 143*, 105889.

Maki, K. (1968). The critical fluctuation of the order parameter in type-II superconductors. *Progress of Theoretical Physics, 39*(4), 897-906.

Malik, B. A., Rather, G. H., Asokan, K., & Malik, M. A. (2021). Study on excess conductivity in YBCO + xAg composites. *Applied Physics A, 127*(4), 294.

Mangelschots, I., Mali, M., Roos, J., Zimmermann, H., Brinkmann, D., Karpinski, J., Kaldis, E., & Rusiecki, S. (1990). Frequency, linewidth and relaxation of Cu NQR signals in the superconductor $YBa_{1.9}Ca_{0.1}Cu_4O_{8\pm y}$. *Journal of the Less Common Metals, 164*, 78-83.

Mannhart, J., Bielefeldt, H., Götz, B., Hilgenkamp, H., Schmehl, A., Schneider, C. W., & Schulz, R. R. (2000). Doping induced enhancement of the critical currents of grain boundaries in high-Tc superconductors. *Physica C: Superconductivity, 341*, 1393-1396.

Manthiram, A., Lee, S., & Goodenough, J. (1988). Influence of Ca on the superconductivity of $Y_{1-x}Ca_xBa_2Cu_3O_{7-\delta}$. *Journal Solid State Chemistry;(United States), 73*(1).

Marquis, C. (2016). This is Advanced Energy: High Temperature Superconducting Transmission. Retrieved from https://blog.advancedenergyunited.org/this-is-advanced-energy-high-temperature-superconducting-transmission

Martinez, M. V. (2014). A Basic Understanding of Scanning Electron Microscopy (SEM) and Energy Dispersive X-ray Detection (EDX). Retrieved from https://www.forensicevidence.net/iama/sem-edxtheory.html

Matsumoto, K., Horide, T., Osamura, K., Mukaida, M., Yoshida, Y., Ichinose, A., & Horii, S. (2004). Enhancement of critical current density of YBCO films by introduction of artificial pinning centers due to the distributed nano-scaled Y_2O_3 islands on substrates. *Physica C: Superconductivity, 412-414*, 1267-1271.

© COPYRIGHT UPM

Matsumoto, Y., Nishimori, T., Yamamoto, H., Nishimura, K., Kamada, K., & Ogata, A. (1998). Calcium doping into $YBa_2Cu_3O_y$ ceramics by the SOED method. *Solid State Ionics, 107*(1-2), 41-45.

Maza, J., & Vidal, F. (1991). Critical-temperature inhomogeneities and resistivity rounding in copper oxide superconductors. *Physical Review B, 43*(13), 10560-10567.

Meissner effect. (2023). Retrieved from http://en.wikipedia.org/wiki/Superdiamagnetism

Mele, P., Matsumoto, K., Horide, T., Ichinose, A., Mukaida, M., Yoshida, Y., Horii, S., & Kita, R. (2007). Incorporation of double artificial pinning centers in $YBa_2Cu_3O_{7-\delta}$ films. *Superconductor Science and Technology*, *21*(1), 015019.

Mikheenko, P., Abell, J., Sarkar, A., Dang, V., Kechik, M. A., Tanner, J., Paturi, P., Huhtinen, H., Babu, N. H., & Cardwell, D. (2010). Self-assembled artificial pinning centres in thick YBCO superconducting films. *Journal of Physics: Conference Series*, *234*(2), 022022.

Miyakawa, N., Zasadzinski, J. F., Ozyuzer, L., Guptasarma, P., Kendziora, C., Hinks, D. G., Kaneko, T., & Gray, K. E. (2000). Superconducting gap and pseudogap from tunneling conductance on $Bi_2Sr_2CaCu_2O_{8+\delta}$ with various oxygen concentration. *Physica C: Superconductivity, 341-348*, 835-838.

Mohadi, R., Anggraini, K., Riyanti, F., & Lesbani, A. (2016). Preparation calcium oxide from chicken eggshells. *Sriwijaya Journal of Environment*, *1*(2), 32-35.

Mohan, R., Singh, K., Kaur, N., Bhattacharya, S., Dixit, M., Gaur, N. K., Shelke, V., Gupta, S. K., & Singh, R. K. (2007). Calcium and oxygen doping in $YBa_2Cu_3O_y$. *Solid State Communications, 141*(11), 605-609.

Mohanta, A., & Behera, D. (2010). Fluctuation induced magneto-conductivity studies in $YBa_2Cu_3O_{7-\delta}$ + $xBaZrO_3$ composite high-T_c superconductors. *Physica C: Superconductivity, 470*(4), 295-303.

Mohanta, A., & Behera, D. (2011). Effect of granularity and inhomogeneity in excess conductivity of $YBa_2Cu_3O_{7-\delta}$ + $xBaTiO_3$ superconductor. *Physica B: Condensed Matter, 406*(4), 877-884.

Mohapatra, U. K., Biswal, R., Behera, D., & Mishra, N. C. (2006). Fluctuation conductivity and inhomogeneity in granular $YBa_2Cu_3O_{7-y}$/Ag composite thick films. *Superconductor Science and Technology*, *19*(6), 635.

Mohomed, K. (2016). Thermogravimetric analysis (TGA) theory and applications. *TA Instruments*, 4-235.

Mukherjee, P. S., Simon, A., Sarma, M. S., & Damodaran, A. D. (1992). Oriented grain growth in $YBa_2Cu_3O_{7-\delta}$ by alkali metals (Li, Na & K) substitution. *Solid State Communications, 81*(3), 253-256.

© COPYRIGHT UPM

Muley, A. B., Chaudhari, S. A., Mulchandani, K. H., & Singhal, R. S. (2018). Extraction and characterization of chitosan from prawn shell waste and its conjugation with cutinase for enhanced thermo-stability. *International Journal of Biological Macromolecules, 111*, 1047-1058.

Murakami, M. (1992). Processing of bulk YBaCuO. *Superconductor Science and Technology, 5*(4), 185.

Murakami, M., Morita, M., Doi, K., & Miyamoto, K. (1989). A new process with the promise of high J_c in oxide superconductors. *Japanese Journal of Applied Physics, 28*(7R), 1189.

Naseri, G. M., Saion, E. B., Abbastabar Ahangar, H., Shaari, A. H., & Hashim, M. (2010). Simple Synthesis and Characterization of Cobalt Ferrite Nanoparticles by a Thermal Treatment Method. *Journal of Nanomaterials, 2010*, 907686.

Naseri, M. G., Saion, E. B., Hashim, M., Shaari, A. H., & Ahangar, H. A. (2011). Synthesis and characterization of zinc ferrite nanoparticles by a thermal treatment method. *Solid State Communications, 151*(14), 1031-1035.

Nazarova, E., Zaleski, A., Zahariev, A., Stoyanova-Ivanova, A., & Zalamova, K. (2004). Effects of substituting calcium for yttrium on the superconducting properties of $YBa_2Cu_3O_z$ bulk samples. *Physica C: Superconductivity, 403*(4), 283-289.

Nazarudin, M., Hamadneh, I., Tan, W., & Zainal, Z. (2011). The effect of sintering temperature variation on the superconducting properties of $ErBa_2Cu_3O_{7-\delta}$ superconductor prepared via coprecipitation method. *Journal of Superconductivity and Novel Magnetism, 24*(5), 1745-1750.

Nedkov, I., & Veneva, A. (1994). Alkali metals impurities influence on the magnetic and electrical properties of YBCO. *Journal of Applied Physics, 75*(10), 6726-6728.

Norazidah, A., Azhan, H., Azman, K., Hidayah, H., & Hawa, J. (2012). Superconducting properties of Calcium substitution in Barium site of porous $YBa_2Cu_3O_7$ ceramics. *Advanced Materials Research, 501*, 294-298.

Ono, A. (1987). A Crystallographic Study on $Ba_2YCu_3O_{7-y}$. *Japanese Journal of Applied Physics, 26*(Part 2, No. 7), L1223-L1225.

Owens, F., & Poole, C. (2002). The new superconductors. In F. J. Owens & C. P. Poole (Eds.), *Electromagnetic Absorption in the Copper Oxide Superconductors* (pp. 31-54). Boston, MA: Springer US.

Pan, V., Cherpak, Y., Komashko, V., Pozigun, S., Tretiatchenko, C., Semenov, A., Pashitskii, E., & Pan, A. V. (2006). Supercurrent transport in Y Ba 2 Cu 3 O 7− δ epitaxial thin films in a dc magnetic field. *Physical Review B, 73*(5), 054508.

Patta, Y., Wesolowski, D., & Cima, M. (2009). Aqueous polymer–nitrate solution deposition of YBCO films. *Physica C: Superconductivity, 469*(4), 129-134.

© COPYRIGHT UPM

Pereira, L. A. A., Junior, P. R., & Jurelo, A. R. (2010). Description of R×T dimensional dependence of YBCO samples with a percolation model. *Physica C: Superconductivity, 470*(2), 159-164.

Pureur, P., Costa, R. M., Rodrigues Jr, P., Schaf, J., & Kunzler, J. V. (1993). Critical and Gaussian conductivity fluctuations in $YBa_2Cu_3O_{7-\delta}$. *Physical Review B, 47*(17), 11420.

Ramli, A., Manhoril, N., & Mansor, W. N. W. (2020). The influences of Cr_2O_3 addition on structural properties of $NdBa_2Cu_3O_{7-\delta}$ Superconductor *Journal of Sustainability Science and Management, 15*(3), 3-9.

Ramli, A., Shaari, A. H., Baqiah, H., Kean, C. S., Kechik, M. M. A., & Talib, Z. A. (2016). Role of Nd_2O_3 nanoparticles addition on microstructural and superconducting properties of $YBa_2Cu_3O_{7-\delta}$ ceramics. *Journal of Rare Earths, 34*(9), 895-900.

Rojas, S. M. P., Uribe Laverde, M. A., Vera López, E., Landínez Téllez, D. A., & Roa-Rojas, J. (2007). Conductivity fluctuation and superconducting parameters of the $YBa_2Cu_{3-x}(PO4)_xO_{7-\delta}$ material. *Physica B: Condensed Matter, 398*(2), 360-363.

Şahan, G., Demir, A., & Gökçe, Y. (2016). Improving certain properties of wool fibers by applying chitosan nanoparticles and atmospheric plasma treatment. *Fibers and Polymers, 17*(7), 1007-1012.

Sahoo, B., Mohapatra, S., Singh, A., Samal, D., & Behera, D. (2019). Effects of CNTs blending on the superconducting parameters of YBCO superconductor. *Ceramics International, 45*(6), 7709-7716.

Sahoo, B., Routray, K. L., Samal, D., & Behera, D. (2019). Effect of artificial pinning centers on YBCO high temperature superconductor through substitution of graphene nano-platelets. *Materials Chemistry and Physics, 223*, 784-788.

Sahoo, B., Singh, A. K., & Behera, D. (2020). Graphene oxide modified superconducting and elastic parameters of YBCO superconductor. *Materials Chemistry and Physics, 240*, 122252.

Sahoo, M., & Behera, D. (2012). Effect of Ferromagnetic Induced Inhomogeneity in Excess Conductivity of YBa2Cu3O7-δ+ x CoFe2O4 Composite. *Journal Materials Science Enggineering, 1*(115).

Sahoo, M., Giri, D., & Behera, D. (2014). Study of structural modification and fluctuation induced electrical conductivity in $YBa_2Cu_3O_{7-y}$ + $BaSnO_3$ superconductor composite. *Journal of Low Temperature Physics, 177*(5), 257-273.

Saito, Y., Noji, T., Endo, A., Higuchi, N., Fujimoto, K., Oikawa, T., Hattori, A., & Furuse, K. (1987). High-T_c superconducting properties in $(Y_{1-x}Tl_x)Ba_2Cu_3O_{7-y}$, $Y(Ba_{1-x}K_x)_2Cu_3O_{7-y}$ and $YBa_2(Cu_{1-x}Mg_x)_3O_{7-y}$. *Physica B+C, 148*(1-3), 336-338.

© COPYRIGHT UPM

Salama, A. H., El-Hofy, M., Rammah, Y. S., & Elkhatib, M. (2015). Effect of magnetic and nonmagnetic nano metal oxides doping on the critical temperature of a YBCO superconductor. *Advances in Natural Sciences: Nanoscience and Nanotechnology, 6*(4), 045013.

Salamati, H., & Kameli, P. (2003). Effect of deoxygenation on the weak-link behavior of $YBa_2Cu_3O_{7-\delta}$ superconductors. *Solid State Communications, 125*(7), 407-411.

Samuels, R. J. (1981). Solid state characterization of the structure of chitosan films. *Journal of Polymer Science, Polymer Physics Edition, 19*(7), 1081-1105.

Sathiya, N. V., Varun Prasath, P., Ravichandran, K., Easwaramoorthy, D., Shahnavaz, Z., Mohammad, F., Al-Lohedan, H. A., Paiman, S., Oh, W. C., & Sagadevan, S. (2020). Schiff-base derived chitosan impregnated copper oxide nanoparticles: An effective photocatalyst in direct sunlight. *Materials Science in Semiconductor Processing, 119*, 105238.

Schmehl, A., Götz, B., Schulz, R. R., Schneider, C. W., Bielefeldt, H., Hilgenkamp, H., & Mannhart, J. (1999). Doping-induced enhancement of the critical currents of grain boundaries in $YBa_2Cu_3O_{7-\delta}$. *EPL (Europhysics Letters), 47*(1), 110.

Selvaraj, S. (2015, 7 April 2015). Thermogravimetric analysis. Retrieved from https://www.slideshare.net/sureshselvaraj108/thermogravimetric-analysis

Slimani, Y., Hannachi, E., Ben Salem, M. K., Hamrita, A., Salem, M. B., & Azzouz, F. B. (2015). Excess conductivity study in nano-$CoFe_2O_4$-added $YBa_2Cu_3O_{7-d}$ and $Y_3Ba_5Cu_8O_{18\pm x}$ superconductors. *Journal of Superconductivity and Novel Magnetism, 28*(10), 3001-3010.

Slimani, Y., Hannachi, E., Ekicibil, A., Almessiere, M. A., & Ben Azzouz, F. (2019). Investigation of the impact of nano-sized wires and particles TiO2 on Y-123 superconductor performance. *Journal of Alloys and Compounds, 781*, 664-673.

Slimani, Y., Hannachi, E., Koblischka-Veneva, A., & Koblischka, M. R. (2024). Excess conductivity analysis of an YBCO foam strut and its microstructure *Preprints*: Preprints.

Smith, E., Schnepp, Z., Wimbush, S. C., & Hall, S. R. (2008). On the suppression of superconducting phase formation in YBCO materials by templated synthesis in the presence of a sulfated biopolymer. *Physica C: Superconductivity, 468*(22), 2283-2287.

Solov'ev, A. L., & Dmitriev, V. M. (2009). Fluctuation conductivity and pseudogap in YBCO high-temperature superconductors (Review). *Low Temperature Physics, 35*(3), 169-197.

Song, C.-L., & Xue, Q.-K. (2017). Cuprate superconductors may be conventional after all. *ArXiv Physics e-Prints, 10*, 129.

Su, H., & Welch, D. O. (2004). The effects of space charge, dopants, and strain fields on surfaces and grain boundaries in YBCO compounds. *Superconductor Science and Technology, 18*(1), 24.

© COPYRIGHT UPM

Sunil, J., Vignesh, J., Vettumperumal, R., Maheswaran, R., & Raja, R. A. A. (2019). The thermal properties of CaO-Nanofluids. *Vacuum, 161*, 383-388.

Superconducting chips to scale up quantum computers and boost supercomputers. (2021). Retrieved from https://siliconsemiconductor.net/article/112853/Superconducting_chips_to_scale_up_quantum_computers_and_boost_supercomputers

Suryanarayana, C. (2011). *Experimental techniques in materials and mechanics*: Crc Press.

Suyama, Y., Matsumoto, M., Kageyama, S., & Sato, I. (1991). *Effect of oxygen deficiency on the superconducting properties of YBCO*. Paper presented at the Advances in Superconductivity III, Tokyo.

Swethavinayagam, K. E. V., Venkatesan, D., & Rebecca, L. J. (2019). Preparation of chitosan nanoparticles and its synergistic effects against gram positive and gram negative microorganisms. *Journal Pure Applied Microbiology, 13*(4), 2317-2324.

Taillefer, L. (2010). Scattering and pairing in cuprate superconductors. *Annual Review of Condensed Matter Physics, 1*.

Talantsev, E., Strickland, N., Wimbush, S., Storey, J., Tallon, J., & Long, N. (2014). Hole doping dependence of critical current density in YBa2Cu3O7− δ conductors. *Applied Physics Letters, 104*(24), 242601.

Tallon, J. L., Benseman, T., Williams, G. V. M., & Loram, J. W. (2004). The phase diagram of high-Tc superconductors. *Physica C: Superconductivity, 415*(1), 9-14.

Tallon, J. L., & Loram, J. W. (2001). The doping dependence of T* – what is the real high-T_c phase diagram? *Physica C: Superconductivity, 349*(1), 53-68.

Tan, C., Awang Kechik, M., Che Dzulkifli, N., Sukor, S., Kamarudin, A., Yap, S., Baqiah, H., Karim, M., Chen, S., & Lim, K. (2023). Effect of concentration of potassium added in $Y_1Ba_2Cu_3O_{7-\delta}$ superconductor by using the thermal treatment method. *AIP Conference Proceedings, 2619*(1).

Thompson, R. S. (1970). Microwave, flux flow, and fluctuation resistance of dirty type-II superconductors. *Physical Review B, 1*(1), 327.

Tomy, C., Malik, S., Prasad, R., Soni, N., & Mohan, A. (1988). The magnetic behaviour of superconducting and nonsuperconducting DyBa2Cu3O7-y and HoBa2Cu3O7-y. *Journal of Physics C: Solid State Physics, 21*(20), 3787.

Trabelsi, Y., Segovia-Chaves, F., & Ben Ali, N. (2023). Tunable defect modes through the (YBCO-Yttria) based on Octonacci photonic quasicrystals. *Results in Physics, 44*, 106176.

Tranquada, J. M., Heald, S., Moodenbaugh, A., & Xu, Y. (1988). Mixed valency, hole concentration, and T c in $YBa_2Cu_3O_{6+x}$. *Physical Review B, 38*(13), 8893.

© COPYRIGHT UPM

Triscone, G., François, M., Genoud, J. Y., Graf, T., Junod, A., Opagiste, C., & Muller, J. (1993). Calcium substitution in the $Y_2Ba_4Cu_7O_{15+\delta}$ superconducting phase. *Journal of Alloys and Compounds*, *196*(1), 235-239.

Van, D. D., & Kes, P. (2010). The discovery of superconductivity. *Physics Today*, *63*(9), 38-43.

Varshney, D., Yogi, A., Dodiya, N., & Mansuri, I. (2011). Alkaline earth (Ca) and transition metal (Ni) doping on the transport properties of $Y_{1-X}Ca_xBa2(Cu_{1-Y}Ni_y)_3O_{7-\delta}$ superconductors. *Journal of Modern Physics, 2011*.

Wang, C., Cook-Chennault, K., & Sastry, A. (2003). Conduction in multiphase particulate/fibrous networks simulations and experiments on Li-ion anodes. *Journal of The Electrochemical Society*, *150*, A385-A397.

Wang, D., Xiao, R., Zhang, H., & He, G. (2010). Comparison of catalytic pyrolysis of biomass with MCM-41 and CaO catalysts by using TGA–FTIR analysis. *Journal of Analytical and Applied Pyrolysis*, *89*(2), 171-177.

West, A. R. (2022). *Solid state chemistry and its applications*: John Wiley & Sons.

Wu, H., Ruan, K., Yin, J., Huang, S., Lv, Z., Li, M., & Cao, L. (2007). Effect of K and Nd substitutions on superconductivity of Bi2223 superconductors. *Superconductor Science and Technology*, *20*(12), 1189.

Wu, J., Emergo, R., Wang, X., Xu, G., Haugan, T., & Barnes, P. (2008). Strong nanopore pinning enhances J_c in $YBa_2Cu_3O_{7-\delta}$ films. *Applied Physics Letters*, *93*(6), 062506.

X-ray Diffraction. (2023). Retrieved from https://www.veqter.co.uk/residual-stress-measurement/x-ray-diffraction

Yamada, Y., Anagawa, K., Shibauchi, T., Fujii, T., Watanabe, T., Matsuda, A., & Suzuki, M. (2003). Interlayer tunneling spectroscopy and doping-dependent energy-gap structure of the trilayer superconductor $Bi_2Sr_2Ca_2Cu_3O_{10+\delta}$. *Physical Review B*, *68*(5), 054533.

Yamin, N. A. M., Zaid, M. H. M., Matori, K. A., Chyi, J. L. Y., Zalamin, S. N. F., Ismail, N. A. N., Chan, K. F., & Effendy, N. (2022). Effect of calcium oxide in the zinc-boro-soda-lime-silica glass matrix by using eggshell waste as calcium source. *Applied Physics A*, *128*(1), 93.

Yan, D.-X., Dai, K., Xiang, Z.-D., Li, Z.-M., Ji, X., & Zhang, W.-Q. (2011). Electrical conductivity and major mechanical and thermal properties of carbon nanotube-filled polyurethane foams. *Journal of Applied Polymer Science*, *120*(5), 3014-3019.

Yawirach, S., Wannasut, P., Boonsong, P., & Watcharapasorn, A. (2023). Effect of sintering time on phase, physical properties, microstructure and thermal conductivity of $Y(Ba_{1-x}La_x)_2Cu_3O_{7-\delta}$ ceramics. *Journal of Physics: Conference Series*, *2431*(1), 012099.

© COPYRIGHT UPM

Yusuf, M., Nur Nabilah, Awang Kechik, M. M., Baqiah, H., Soo Kien, C., Kean Pah, L., Shaari, A. H., Wan Jusoh, W. N. W., Sukor, A., Izzati, S., & Mousa Dihom, M. (2019). Structural and superconducting properties of thermal treatment-synthesised bulk $YBa_2Cu_3O_{7-\delta}$ superconductor: effect of addition of SnO_2 nanoparticles. *Materials*, *12*(1), 92.

Zhang, J., Xia, W., Liu, P., Cheng, Q., Tahirou, T., Gu, W., & Li, B. (2010). Chitosan modification and pharmaceutical/biomedical applications. *Marine Drugs*, *8*(7), 1962-1987.

Zhang, Z. L., Wimbush, S. C., Kursumovic, A., Suo, H., & MacManus Driscoll, J. L. (2013). Role of the organic matrix in the biopolymer-mediated synthesis of platelike YBCO. *Advanced Materials Research*, *699*, 268-272.

© COPYRIGHT UPM